

UC San Diego

UC San Diego Previously Published Works

Title

Defining the proximal interaction networks of Arf GTPases reveals a mechanism for the regulation of PLD1 and PI4KB

Permalink

<https://escholarship.org/uc/item/90m6q5tk>

Journal

The EMBO Journal, 41(17)

ISSN

0261-4189

Authors

Li, Fu-Long

Wu, Zhengming

Gao, Yong-Qi

et al.

Publication Date





2022-09-01

DOI

10.15252/emj.2022110698

Peer reviewed

Defining the proximal interaction networks of Arf GTPases reveals a mechanism for the regulation of PLD1 and PI4KB

Fu-Long Li¹, Zhengming Wu¹, Yong-Qi Gao² , Forrest Z Bowling³, J Matthew Franklin¹, Chongze Hu⁴, Raymond T Suhandynata², Michael A Frohman⁵, Michael V Airola³ , Huilin Zhou²  & Kun-Liang Guan^{1,*} 

Abstract

The Arf GTPase family is involved in a wide range of cellular regulation including membrane trafficking and organelle–structure assembly. Here, we have generated a proximity interaction network for the Arf family using the miniTurboID approach combined with TMT-based quantitative mass spectrometry. Our interactome confirmed known interactions and identified many novel interactors that provide leads for defining Arf pathway cell biological functions. We explored the unexpected finding that phospholipase D1 (PLD1) preferentially interacts with two closely related but poorly studied Arf family GTPases, ARL11 and ARL14, showing that PLD1 is activated by ARL11/14 and may recruit these GTPases to membrane vesicles, and that PLD1 and ARL11 collaborate to promote macrophage phagocytosis. Moreover, ARL5A and ARL5B were found to interact with and recruit phosphatidylinositol 4-kinase beta (PI4KB) at trans-Golgi, thus promoting PI4KB's function in PI4P synthesis and protein secretion.

Keywords ARL11; ARL5; Phagocytosis; PI4KB; PLD1

Subject Categories Membrane & Trafficking; Proteomics

DOI 10.15252/emboj.2022110698 | Received 17 January 2022 | Revised 25 May 2022 | Accepted 3 June 2022 | Published online 17 July 2022

The EMBO Journal (2022) 41: e110698

See also: [D Barneda et al](#) (September 2022)

Introduction

The Ras superfamily, which is subdivided into the Ras, Rho, Rab, Arf, and Ran subfamilies, plays key roles in physiological processes such as signal transduction, cytoskeletal remodeling, membrane trafficking, and secretory and endocytic pathways (Rojas *et al*, 2012). The Arf subfamily is composed of 29 proteins that are

best known for regulating membrane trafficking, and secretory and endocytic pathways (Gillingham & Munro, 2007; Mizuno-Yamasaki *et al*, 2012). Arf proteins act as molecular switches, cycling between inactive GDP-bound and active GTP-bound states to regulate the activity or localization of their effector proteins (Donaldson & Jackson, 2011). Dysregulation of Arf GTPases or their regulators can result in various diseases; for example, mutations of *ARL13B* cause Joubert syndrome, and mutations of *ARL6* cause Bardet–Biedl syndrome, emphasizing the physiological importance of the Arf family (Li *et al*, 2012; Seixas *et al*, 2013; Casalou *et al*, 2020).

Arf family proteins were initially identified and defined to be essential for ADP-ribosylation of the heterotrimeric Gs protein by cholera toxin (Kahn & Gilman, 1986). Six closely related proteins denoted Arf1 to Arf6 were found to have this activity (Arf2 is absent in humans). The Arf family also contains a larger subgroup of small G proteins sharing high structural similarity but without the ADP-ribosylation cofactor activity, including the secretion-associated RAS-related (Sar) proteins Sar1, Arf-like (Arl) proteins, Arf-related protein 1 (Arfrp1), and the tripartite motif-containing protein 23 (Trim23) (Gillingham & Munro, 2007). Arf1, Arf6, and Sar1 are the best-characterized members of the Arf family, while others, including ARL5A/5B, ARL11, and ARL14, remain less well understood. The repertoire of Arf effectors is large and incomplete. Meanwhile, the exact specificity of effectors or regulators, and whether they are selectively or generally regulated by Arf proteins, remains important open questions. Furthermore, prior studies of Arf family members have in general been conducted on single or small groups of family members under varying experimental conditions or were focused on a single pathway. Thus, the fragmented understanding of the Arf family warrants a systematic search for a complete effector network to provide a comprehensive view of Arf family function and regulation.

Proximity labeling coupled with mass spectrometry has emerged as a powerful approach to identify protein–protein interactions, especially for capturing weak and transient protein–protein

1 Department of Pharmacology and Moores Cancer Center, University of California San Diego, La Jolla, CA, USA

2 Department of Cellular and Molecular Medicine, University of California San Diego, La Jolla, CA, USA

3 Department of Biochemistry and Cell Biology, Stony Brook University, Stony Brook, NY, USA

4 Department of Nanoengineering, Program of Materials Science and Engineering, University of California San Diego, La Jolla, CA, USA

5 Department of Pharmacological Sciences, Stony Brook University, Stony Brook, NY, USA

*Corresponding author. Tel: +1 858 822 7945; E-mail: kuguan@ucsd.edu

interactions (Roux *et al*, 2018; Choi & Rhee, 2022). TurboID/mini-Turbo are directed evolution-engineered biotin ligases that generate the biotin-AMP to chemically label proximal proteins, which can then be purified by streptavidin beads (Branon *et al*, 2018). Compared with the initial proximity labeling enzyme BirA-R118S used in BioID, TurboID/miniTurbo display higher activity with much shorter labeling time, therefore leading to less background signal and higher sensitivity. The tandem mass tag (TMT) covalently labels peptides, which can then be identified by high-resolution mass spectrometry (Thompson *et al*, 2003). Isotopically distinct TMT labeling allows quantification of the relative abundance of each protein across multiple samples (Zhang & Elias, 2017). By combining these methods, we systematically mapped the ARF-family proximal protein interactome. We established the regulation and function of phospholipase D1 (PLD1) by ARL11/ARL14 and phosphatidylinositol 4-kinase B (PI4KB) by ARL5A/ARL5B.

Results

An interaction network of the Arf family identified by miniTurboID and mass spectrometry

Arf proteins execute their functions by physical interaction with downstream effectors. However, these interactions are transient and often take place on organelle membranes, making them difficult to be captured by standard copurification approaches. Here, we used miniTurboID with TMT-based mass spectrometry to systematically define Arf family interacting proteins (Fig 1A). Constitutively active mutants of Arf family GTPases were generated and fused with miniTurboID to identify activity-dependent downstream effectors. Unlike the Ras, Rab, and Rho subfamily, small GTPases that are isoprenylated at the C-terminus, Arf subfamily members are usually modified by myristoylation at their N-termini (Prakash & Gorfe, 2017). We thus placed the miniTurbo biotin ligase at the C-terminus of the Arf proteins. HEK293 cells were chosen in this study because they have been used widely in many proteomic studies and this would enable optimal comparison with published data (Antonicka *et al*, 2020; Go *et al*, 2021; Huttlin *et al*, 2021). The miniTurbo Arf fusions were stably expressed in HEK293A cells as confirmed by Western blotting (Appendix Fig S1A). The expression levels of ARF1-miniTurbo-HA and ARF6-miniTurbo-HA, as examples, were comparable to those of the endogenous GTPases (Appendix Fig S1B).

A total of 25 Arf members were screened using miniTurboID and TMT-MS (Fig 1B). MiniTurbo-HA without GTPase fusion was included as a control in each set of MS analysis. We failed to obtain clones of two GTPases ARL5C and ARL13A, while protein expression of two other GTPases ARL4A and ARL9 was not detected even though DNA sequencing verified the constructs. The proximity labeling condition was optimized to obtain efficient labeling and low background biotinylation. For example, 1 μ M biotin efficiently labeled the ARF1 effectors COPB1 and AP3B1, while higher concentrations of biotin (such as 10 μ M or higher) increased the global biotinylation dramatically and labeled COPB1 and AP3B1 in the miniTurbo negative control (Appendix Fig S1C). We found that labeling with 1 μ M biotin for 15 min was optimal. Biotinylated proteins were captured from cell lysates using streptavidin beads, followed by on-bead trypsin digestion. The resulting peptides from

four samples and one control were chemically conjugated to isotopically distinct TMT labels before being pooled together for each HPLC-MS analysis. The enrichment fold of protein identified was normalized against the background. Two biologically independent replicas were performed for each ARF GTPase, and the final enrichment fold was the mean value of these two replicas. Correlation analysis of these replicas for each GTPase indicated there is a strong or moderate positive correlation between two replicas in the majority of GTPase datasets (Appendix Fig S1D and E). We detected 1,667 interactions between the GTPase baits and the interactors filtered by the significant test (Datasets EV1–EV25) (Cox & Mann, 2008). A comparison of our proximal interactome with the previously reported protein, genetic, and chemical Arf interactomes revealed that the overlap was low, with only 1.9% of our hits being listed in BioGRID (<https://thebiogrid.org>; Appendix Fig S1F), which is consistent with other similar BioID studies (Couzens *et al*, 2013; Gupta *et al*, 2015; Youn *et al*, 2018; Bagci *et al*, 2020). Our results suggest that miniTurboID represents a complementary approach to identify protein–protein interactions for the ARF family GTPases.

Proximity interactions reveal a potential effector landscape of Arf GTPases

To explore the functional landscape of Arf interacting proteins, we first delineated gene ontology (GO) terms associated with these proximal proteins (Fig 2A). The most significant term associated with the Arf family proximal interaction network concerns pathways related to the cellular transport and macromolecule localization, such as vesicle-mediated transport, followed by pathways involved in cellular organelle assembly such as endomembrane system organization (Fig 2A). These highly enriched pathways of Arf proximal network recapitulate the known function of the Arf family (Donaldson & Jackson, 2011; Mizuno-Yamasaki *et al*, 2012), thus confirming the quality of our interactome. Meanwhile, the other significant terms may reveal additional function association with the Arf family, such as viral and nucleic acid process (Fig 2A), which was reported in sporadic studies (Belov *et al*, 2007; Lanke *et al*, 2009; Nishikiori *et al*, 2011; Iglesias *et al*, 2015).

As the Arf family is mainly known to regulate membrane-associated secretory and endocytic pathways, the proximity proteins that were identified by our experiments and known to be involved in vesicle coating and membranal lipid metabolism were analyzed and compared across the 25 Arf family members (Fig 2B). SAR1A/B, which is one of the five core components of the COPII complex, exclusively identified the majority of the components related to the COPII complex (SEC23A/B, SEC24A/B/C/D, SEC31A, SEC23IP, SEC22B, TFG, and SEC16A), which coats vesicle transporting proteins from the rough ER to the Golgi (Barlowe *et al*, 1994). Intriguingly, INPP5E (Inositol polyphosphate 5-phosphatase B) was also labeled. INPP5E is best known for its roles in endocytosis and receptor recycling (Noakes *et al*, 2011) but has also been linked to the early secretory pathway (Williams *et al*, 2007). Since no interaction between INPP5E and SAR1A/B has previously been reported, this finding provides an example of the novel leads generated from our experimental approach.

In contrast to the SAR1A/B findings, the ARF1-ARF6 miniTurbo fusion proteins selectively enriched many components of the COPI complex (COPB, COPD, COPG1, COPG2, and COPZ1; Fig 2B), which

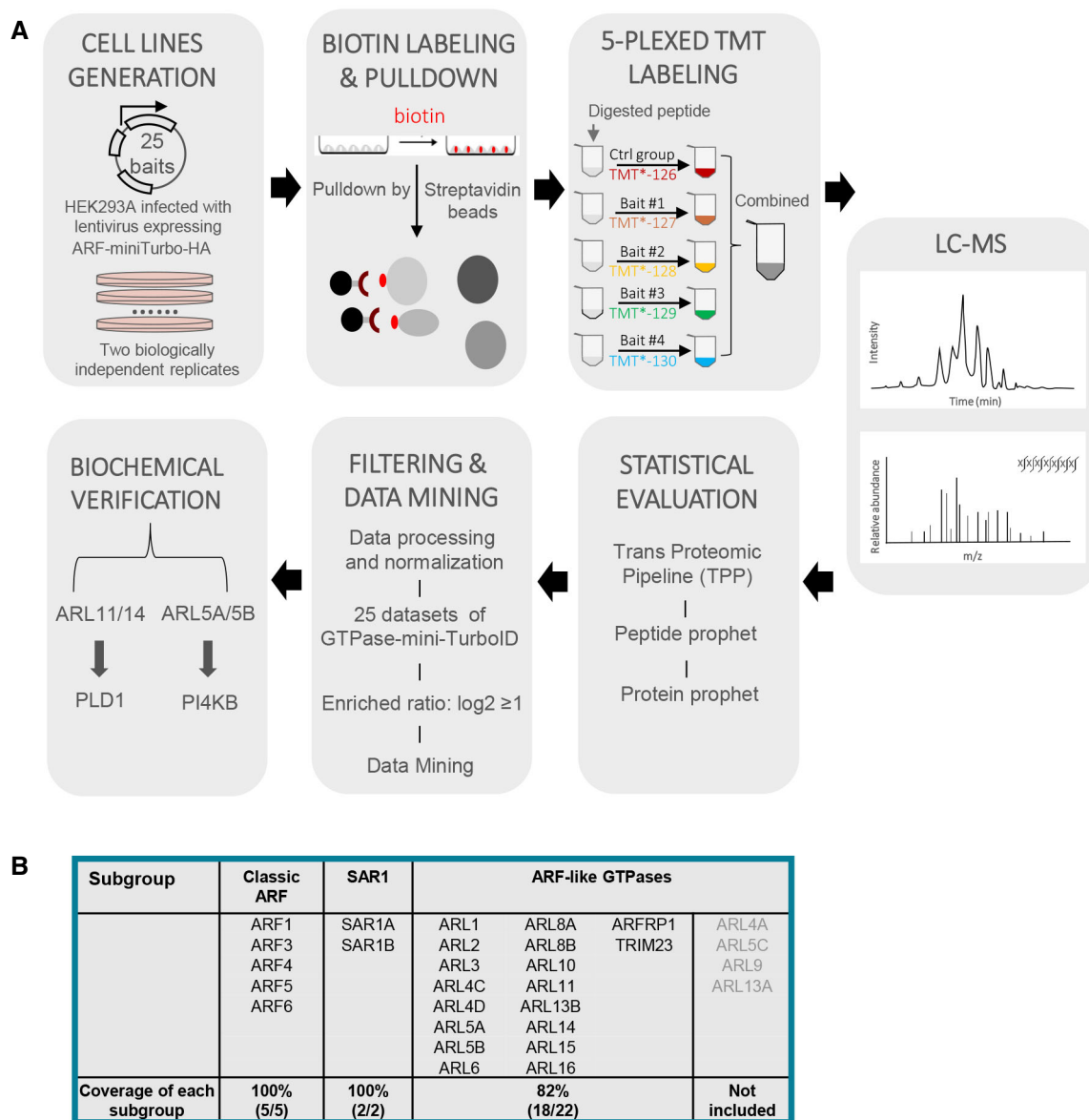


Figure 1. Systematic mapping of ARF family proximal interaction network by miniTurboID-TMT-MS.

A Workflow used to generate ARF family proximal interaction network. This includes the construction of ARF-miniTurbo-HA vectors, generation of cell lines stably expressing the bait, biotin labeling, streptavidin purification, peptide digestion, TMT-coupled quantitative mass spectrometry, peptide identification with TPP, statistical evaluation, data mining, and biochemical verification.

B A list of ARF family GTPases included or not included in this study.

transports proteins from the *cis* end of the Golgi complex back to the rough ER (Duden, 2003; Arakel & Schwappach, 2018). Analogous to Sar1 and COPII, the Arfs are key components in forming COPI-coated vesicles (Pucadyil & Schmid, 2009), further validating our approach. The Arfs also labeled many members of adaptor protein complexes (AP3B1, AP3D1, AP3S1, AP3S2, and AP4E1; Fig 2B), which recognize and concentrate cargo proteins into vesicular carriers (Park & Guo, 2014; Sanger *et al.*, 2019). The Arf proteins are well known to interact with AP-3 and AP-4 (Park & Guo, 2014), and as well are known to interact with AP-1, which was not labeled in our study. However, EPN4 (EpsinR), which does interact with AP-1

(Wasiak *et al.*, 2002), was identified as very strong hit (Fig 2B). Since EPN4 does not interact with AP-3 or -4, this finding suggests a possibly additional level of complexity to the completeness of proximal labeling by miniTurboID fusion proteins.

These observations further confirm the quality and specificity of our experimental approaches. Notably, the majority of the protein interactions identified by the miniTurboID-TMT-MS in our experiments have not been reported (Appendix Fig S2A and Datasets EV1–EV25). For example, phospholipase D1 (PLD1) was identified as a proximity protein for both ARL11 and ARL14, and phosphatidylinositol 4-kinase B (PI4KB) was identified as a proximity

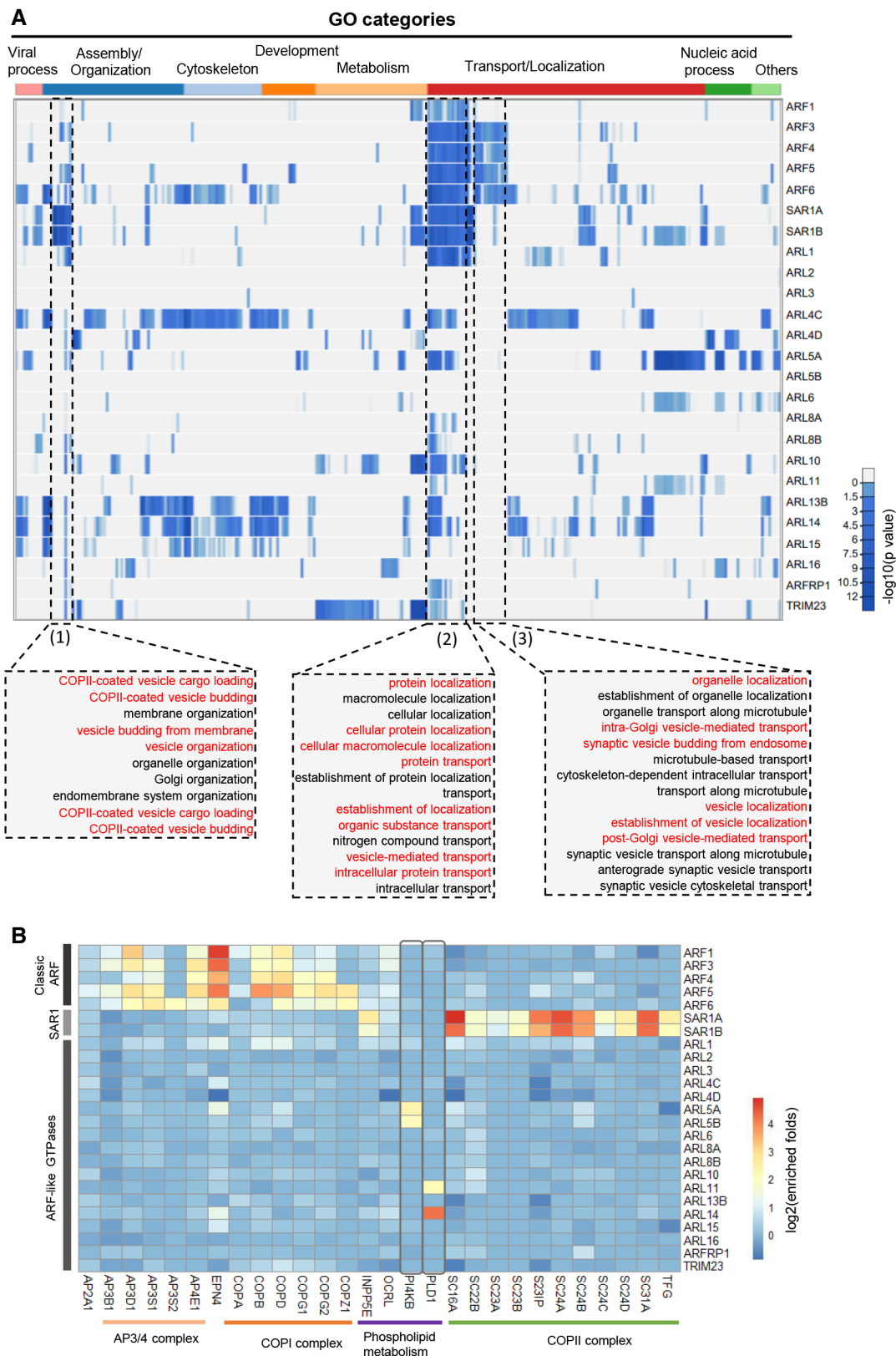


Figure 2.

Figure 2. Functional landscape of the ARF family proximal interaction network.

- A Heatmap of the most significant terms associated with the ARF family proximal interaction proteins identified in this study. Representative pathways were listed in the lower dotted box and highlighted in red.
- B Heatmap of proteins involved in vesicle coating and phospholipid metabolism identified in this study. Prey proteins belonging to the specific pathways are shown on the bottom.

interactor for ARL5A and ARL5B (Fig 2B). To validate our findings, we characterized these interactions and their functional significance in detail below.

PLD1 binds to and colocalizes with ARL11/14

PLD1 hydrolyzes the headgroup of phosphatidylcholine (PC), the most abundant membrane phospholipid, to produce choline and phosphatidic acid (PA) (Jenkins & Frohman, 2005). PLD1 has been extensively studied for its role in signal transduction, membrane trafficking, endocytosis and exocytosis (Jang et al, 2012; Frohman, 2015), and human mutations in PLD1 result in congenital heart disease (Lahrouchi et al, 2021). PLD1 was labeled uniquely by the ARL11 and ARL14 miniTurboID fusion proteins (Figs 2B and 3A). Protein homology comparison showed that ARL11 and ARL14 are more closely related to each other than to any other ARL subfamily member (Appendix Fig S3A; Rojas et al, 2012). ARL11, also known as ARLTS1, is best studied for its variants associated with elevated risk for breast, prostate, and colorectal familial cancer (Calin et al, 2005; Siltanen et al, 2008), but the cellular functions of ARL11/14 remain largely understudied.

PLD1 has long been studied as an effector of Arf1 and Arf6 (Jenkins & Frohman, 2005). The Arfs are potent stimulators of PLD1 activity, but their physical interaction has been difficult to demonstrate, and we did not detect PLD1 in our experiments when these GTPases were used as baits (Appendix Fig S3B). PLD1 is also activated by the RhoA and related cdc42 small GTPases, for which physical interaction has been demonstrated (Bowling et al, 2020). However, RhoA and cdc42 miniTurboID fusion proteins also did not label PLD1

(Appendix Fig S3B), suggesting infrequent proximity to them at best. We compared the interaction between GTP-bound mutant forms of ARF1, ARF6, RHOA, ARL11, and ARL14 with PLD1 by co-immunoprecipitation. We found that the interaction of PLD1 with ARL11 and ARL14 was much stronger than with ARF1 and ARF6, and RHOA showed no interaction (Fig 3B), consistent with our mass spectrometry results (Fig 3A and Appendix Fig S3B). Semi-endogenous co-immunoprecipitation experiment revealed an interaction between the ectopically expressed HA-ARL11 and endogenous PLD1 (Appendix Fig S3C). We next examined the subcellular localization of these proteins to corroborate the co-IP data. PLD1 is known to localize on vesicular structures such as endosomes and lysosomes. Strong colocalization of ARL11 or ARL14 with PLD1 was observed with most of the PLD1 puncta overlapping the ARL11 or ARL14 puncta (Fig 3C and D). In contrast, ARF1 was observed mainly in the perinuclear region and showed only partial colocalization with PLD1. ARF6 showed plasma membrane enrichment and very weak colocalization with PLD1, and RHOA was relatively diffusely localized in the cytoplasm and displayed only weak colocalization with PLD1. The subcellular colocalization data were consistent with the relative strength of interaction detected by mini-TurboID and co-immunoprecipitation, thus supporting a model in which ARL11/14 interacts strongly with PLD1.

We assessed whether GTP binding might regulate the interaction of ARL11 with PLD1. Co-immunoprecipitation showed that PLD1 preferentially interacted with the GTP-bound ARL11 mutant (ARL11^{Q67L}) over the GDP-bound ARL11 mutant (ARL11^{T26N}) (Fig 3E). Furthermore, ARL11^{Q67L} but not ARL11^{T26N} colocalized with PLD1, and ARL11^{WT} partially colocalized with PLD1 (Fig 3F and G),

Figure 3. PLD1 is an ARL11- and ARL14-interacting protein.

- A PLD1 is enriched by ARL11 and ARL14 miniTurboID. A graph showing proteins that are enriched with ARL11 or ARL14 compared with the vector. The result is presented as the mean of two biologically independent samples.
- B Interaction between PLD1 and ARL11/14 is stronger than between ARF1/6 and RhoA. Flag-tagged PLD1 was co-expressed with HA-tagged GTP-bound mutants of small GTPases in HEK293A cells as indicated. PLD1 was immunoprecipitated with Flag beads, and the coprecipitated small GTPases were detected with an HA antibody. The result is representative of three biologically independent experiments.
- C ARL11/14 colocalize with PLD1. Flag-tagged PLD1 was co-expressed with HA-tagged GTP-bound mutants of small GTPases in HEK293A cells as indicated. After 24 h, cells were fixed with 4% paraformaldehyde, followed by incubation with anti-Flag and anti-HA primary antibodies. The Flag and HA antibodies were detected by anti-mouse and anti-rabbit secondary antibodies, respectively. DAPI (blue) was used for DNA staining. Scale bars: 10 μ m. The result is representative of two biologically independent experiments.
- D Mander's overlap coefficient of (C). Mander's overlap coefficient was calculated using JACoP plug-in in ImageJ. Mean \pm standard deviation (SD), $n = 6$ technically independent samples.
- E PLD1 preferentially binds to the GTP form, not the GDP form, of ARL11. Flag-tagged PLD1 was co-expressed with HA-tagged ARL11^{Q67L} (GTP-form) or ARL11^{T26N} (GDP-form) mutant in HEK293A cells. The result is representative of two biologically independent experiments.
- F The subcellular colocalization of ARL11 with PLD1 is GTP-dependent. HA-tagged GTP-bound ARL11^{Q67L}, wild-type ARL11, or GDP-bound ARL11^{T26N} was co-expressed with Flag-tagged PLD1. After 24 h, cells were fixed, followed by incubation with anti-Flag and anti-HA primary antibodies. DAPI (blue) was used for DNA staining. Scale bars: 10 μ m. The result is representative of three biologically independent experiments.
- G Mander's overlap coefficient of (F). Mander's overlap coefficient was calculated using JACoP plug-in in ImageJ. Mean \pm SD; one-way ANOVA, $n = 6$ technically independent samples, * $P < 0.05$.

Source data are available online for this figure.

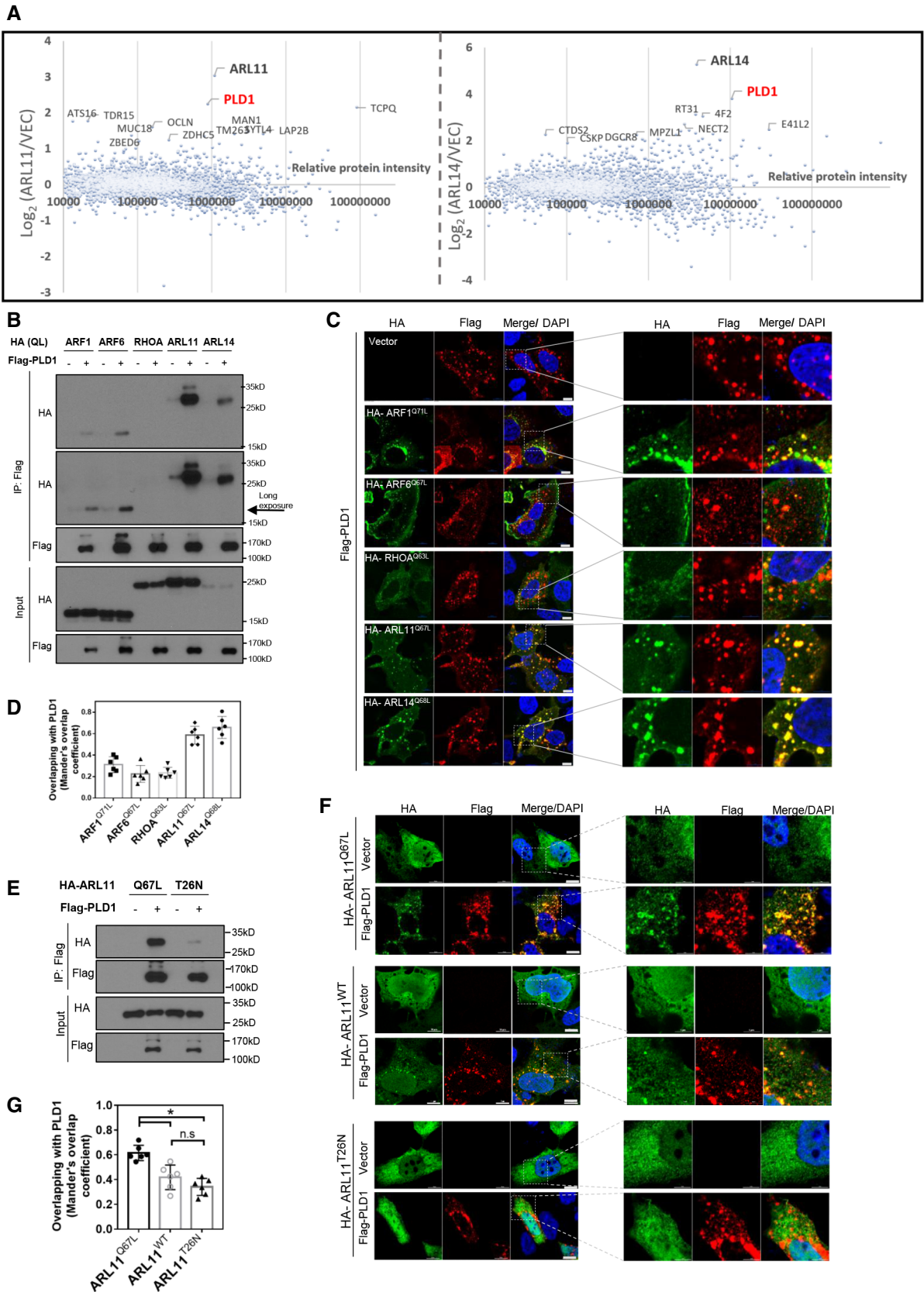


Figure 3.

confirming that the ARL11 interaction with PLD1 is GTP-dependent. Interestingly, ARL11 was diffusely localized in the cytoplasm in the absence of PLD1 co-expression (Fig 3F). Similarly, the PLD1 binding-defective ARL11^{T26N} mutant was also diffusely localized, suggesting that PLD1 may function to recruit GTP-bound ARL11 to subcellular membrane vesicles.

The loop region of PLD1 is required for interaction with and activation by ARL11/14

PLD1 is composed of N-terminal PX and PH lipid-binding domains, a central catalytic domain that includes two conserved HxKxxxxD (HKD) catalytic motifs separated by a loop region of unknown function, and a C-terminal region also critical for enzymatic activity (Fig 4A) (Liu et al, 2001; Selvy et al, 2011). To map the region in PLD1 responsible for interaction with ARL11, we generated various PLD1 deletion constructs and tested their interaction with ARL11 by co-immunoprecipitation. We found that the central loop region is critical for interaction with ARL11 (Fig 4B). Colocalization experiments confirmed that loss of the loop region in PLD1 disrupted the colocalization with ARL11 and ARL14 (Fig 4C and D and Appendix Fig S4A and B).

We then investigated whether PLD1 can be directly activated by ARL11/14. We performed an *in vitro* PLD1 activity assay with purified ARF11/14 and PLD1 using a previously described assay (Bowling et al, 2020). The results showed that PLD1 was activated fourfold and eightfold by ARL11 and ARL14, respectively, while ARF1 and ARF6 generated much weaker activation and RHOA did not stimulate PLD1 (Fig 4E). Importantly, deletion of the loop region, which is not required for lipase activity (Sung et al, 1999), largely diminished PLD1 activation by ARL11 and ARL14 without affecting the weaker activation driven by Arf1 and Arf6 that do not require the loop region (Fig 4E) (Sung et al, 1999). Our results demonstrate that PLD1 is a downstream effector of and can be activated by ARL11 and ARL14. Furthermore, the loop region within PLD1 appears to serve regulatory function by interacting with ARL11 and ARL14 (Fig 4F).

ARL11 acts through PLD1 to promote phagocytosis

Our findings raised an issue of the biological significance of PLD1's interaction with ARL11 and ARL14. The Human Protein Atlas dataset showed that the mRNA expression of ARL11 is enriched in lymphoid tissues and that ARL14 is enriched in gallbladder, intestine, and stomach tissues (Uhlen et al, 2010; Uhlen et al, 2015). Analysis of a single-cell RNA-sequencing dataset revealed that ARL11 expression is primarily present in Kupffer cells, Hofbauer cells, and macrophages, all of which function as phagocytosis executors in the corresponding tissues (Fig 5A and Appendix Fig S5A). In addition, pharmacological inhibition or siRNA-mediated silencing of PLD1 has been reported to suppress phagocytosis (Corrotte et al, 2006; Ali et al, 2013). Collectively, these observations inspired us to test the function of ARL11 in macrophage phagocytosis and the possible involvement of PLD1.

THP-1 are human monocytes derived from acute monocytic leukemia and can be differentiated into macrophages *in vitro*. Three ARL11 knockout cell pools were generated using three independent CRISPR/Cas9 guide RNAs and were verified by immunoblotting

(Fig 5B). The THP-1 cells were induced to differentiate into macrophages by phorbol-12-myristate-13-acetate (PMA), and phagocytosis assays were performed using fluorescence zymosan particles. We observed that deletion of ARL11 inhibited particle uptake in all three ARL11-knockout THP1-differentiated macrophage pools (Fig 5C). Stable overexpression of the active GTP-form ARL11^{Q67L} increased phagocytosis, whereas the inactive GDP-form ARL11^{T26N} did not (Fig 5D–F). To test the functional relationship with PLD1, we generated two PLD1 knockout THP-1 cell pools with independent guide RNAs (Fig 5G). In the wild-type cells, HA-tagged ARL11^{Q67L} showed puncta staining and was avoided in the nucleus. PLD1 knockout resulted in more diffused ARL11^{Q67L} distribution, particularly with increased nuclear localization (Appendix Fig S5C and D), indicating that PLD1 may influence ARL11 localization to cellular vesicles. Importantly, we found that while ARL11^{Q67L} was able to stimulate phagocytosis in wild-type THP-1 cells, PLD1 deletion abolished the ARL11^{Q67L}-stimulated phagocytosis (Fig 5H and I). Taken together, our findings show that ARL11 acts through PLD1 to stimulate macrophage phagocytosis.

ARL5A/5B recruit PI4KB to increase local PI4P levels

Phosphatidylinositol 4-kinase beta (PI4KB) was identified as a putative interacting protein for ARL5A and ARL5B (Fig 2B). PI4KB phosphorylates phosphatidylinositol (PI) at the 4-position of the inositol ring to generate the membrane lipid phosphatidylinositol 4-phosphate (PI4P), which is a key signaling molecule in cellular regulation. PI4P on the Golgi membrane promotes the recruitment of COPI complexes and clathrin adaptor protein to stimulate the biogenesis of trafficking vesicles that regulate cellular processes such as membrane trafficking from Golgi-to-cell surface, sphingolipid transport, protein secretion, and virus entry and replication (Santiago-Tirado & Bretscher, 2011). PI4KB is tightly controlled through interactions with its regulators (Boura & Nencka, 2015). PI4KB has been reported to be activated by ARF1 (Godi et al, 1999). However, a direct ARF1-PI4KB interface has not been found, which suggests that the interaction may be indirect. Besides ARF1, PI4KB has also been found to interact with and recruit RAB11 to the Golgi complex to regulate biosynthetic membrane transport (de Graaf et al, 2004). The human genome has two closely related ARL5 paralogues (ARL5A and ARL5B), and both ARL5A and ARL5B localize to the trans-Golgi network. ARL5 has been reported to be involved in retrograde traffic from endosomes to the Golgi apparatus by interaction with the Golgi-associated retrograde protein GARP complex (Rosa-Ferreira et al, 2015).

Besides ARL5A/5B and RAB14, which showed the strongest interaction with PI4KB, RAB11B weakly enriched PI4KB, whereas RAB11A and ARF1 did not enrich PI4KB by a miniTurboID screening of the Ras superfamily members (Fig 6A). We compared the interaction of PI4KB with ARF1, RAB11A, RAB11B, ARL5A, ARL5B, and RAB14 with PI4KB by co-immunoprecipitation. Consistent with the miniTurboID results, we found that the interactions of PI4KB with ARL5A and ARL5B were stronger than with the other small GTPases (Fig 6B). As a negative control, ARL11 showed no coprecipitation with PI4KB. Immunoprecipitation with anti-PI4KB antibody confirmed the interaction between endogenous PI4KB and ARL5A/B (Appendix Fig S6A). We compared the binding of PI4KB with the GTP-bound form ARL5B^{Q70L} and the GDP-bound form

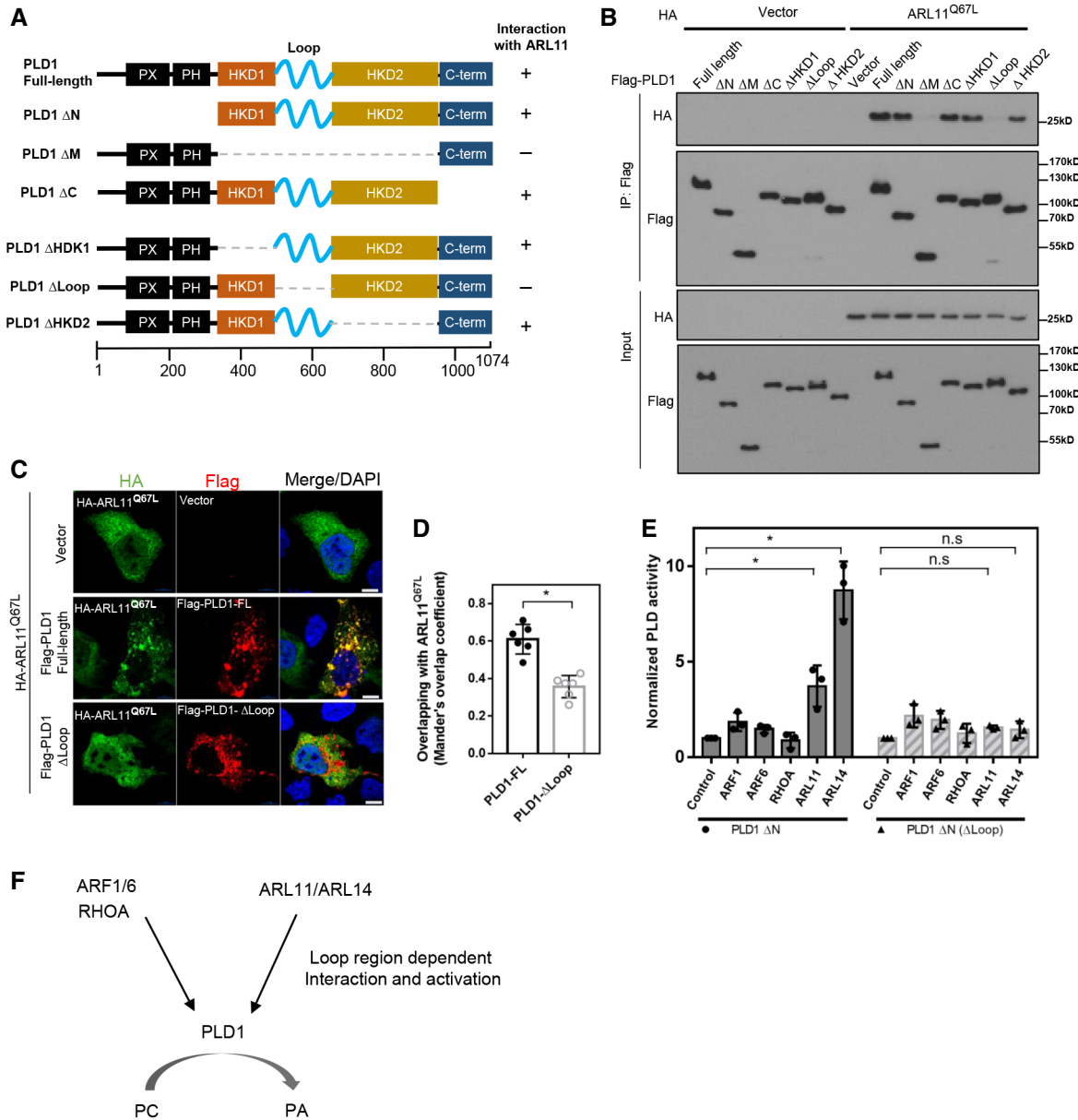


Figure 4. Loop region of PLD1 is required for interaction with and activation by ARL11.

A Schematic representation of the full-length PLD1 and various truncations. Δ N, deletion of the N-terminal PX and PH lipid-binding domain (1-329aa); Δ M, deletion of the central catalytic domain (330-967aa); Δ C, deletion of the C-terminal domain (968-1074aa); Δ HDK1, deletion of the HDK1 domain (330-500aa); Δ Loop, deletion of the loop region (501-642aa); and Δ HDK2, deletion of the HDK2 domain (643-967aa). “+” denotes positive interaction with ARL11, and “-” denotes no interaction.

B The loop region of PLD1 is required for the interaction between ARL11 and PLD1. Flag-tagged full-length or truncations of PLD1 were co-expressed with HA-tagged ARL11^{Q67L}, PLD1 was immunoprecipitated with Flag beads, and ARL11 that associated with it was detected with an HA antibody. The result is representative of two biologically independent experiments.

C Deletion of the loop region disrupts the PLD1 and ARL11 colocalization. Flag-tagged full-length or Δ Loop truncation of PLD1 was co-expressed with HA-tagged ARL11^{Q67L}. After 24 h, cells were fixed with 4% paraformaldehyde, followed by incubation with anti-Flag and anti-HA primary antibodies. DAPI (blue) was used for DNA staining. Scale bars: 10 μ m. The result is representative of three biologically independent experiments.

D Mander's overlap coefficient of (j). Mander's overlap coefficient was calculated using JAcOP plug-in in ImageJ. Mean \pm SD; two-tailed Student's *t*-test, *n* = 6 technically independent samples, **P* < 0.05.

E ARL11 and ARL14 stimulation of PLD1 activity is dependent on the loop region. The *in vitro* activity assay was performed using PLD1 protein of catalytic domain (PLD1 Δ N) with or without the loop region. Details were described in the Methods part. Data are presented as mean \pm SD of three biologically independent samples. One-way ANOVA; n.s. denotes not significant, **P* < 0.05.

F A model of PLD1 activation by GTPases. In contrast to ARF1/6 and RHOA, ARL11/14 stimulate PLD1 activity in a manner dependent on the loop region.

Source data are available online for this figure.

ARL5B^{T30N}. PI4KB preferentially bound to the GTP form of ARL5B, indicating that the interaction is ARL5B activity-dependent (Fig 6C).

Next, we performed subcellular localization to collaborate the protein-protein interaction data. ARL5A^{Q70L} and ARL5A^{WT} colocalized with PI4KB, especially in the perinuclear regions that are likely to be Golgi (Fig 6D). Consistent with the co-immunoprecipitation data, the GTP-bound mutant of ARL5A showed stronger colocalization with PI4KB than the GDP-bound mutant. Interestingly, the GDP-bound mutant ARL5A^{T30N} caused a more diffused subcellular

distribution of PI4KB (Fig 6D). We speculate that the GDP-bound mutant ARL5A/5B may function as dominant negatives to inhibit the endogenous ARL5A/5B, thus reducing PI4KB Golgi localization. We examined the colocalization of ARL5A^{Q70L} with different Golgi markers: GM130 (cis-Golgi), Giantin (cis/medial-Golgi), and TGN46 (trans-Golgi). We observed that ARL5A displayed a stronger overlap with TGN46 than with GM130 or Giantin, indicating that ARL5A localizes with the trans-Golgi network (Appendix Fig S6B). We then determined the effect of ARL5A/5B on PI4KB localization. Double

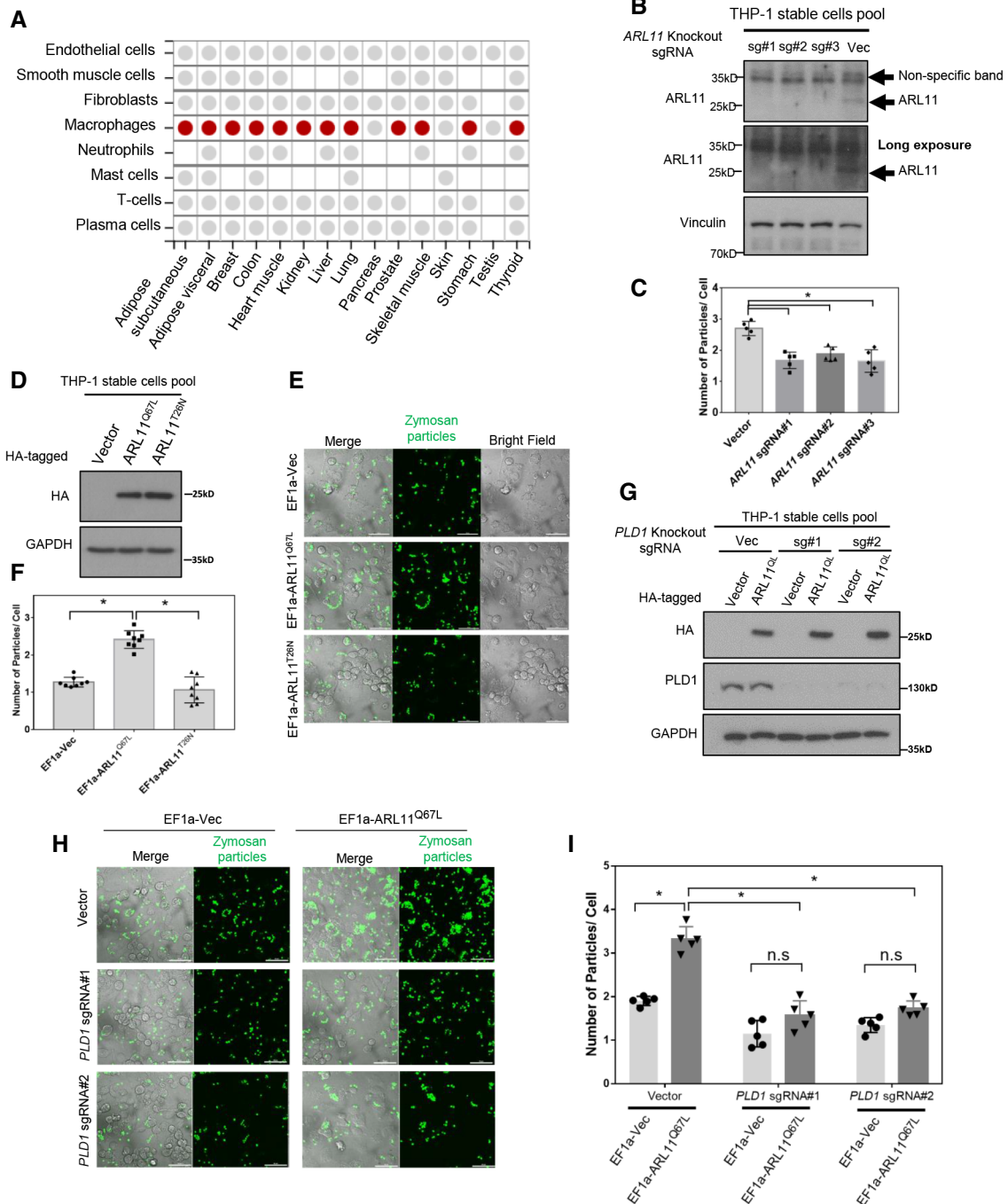


Figure 5.

Figure 5. ARL11 requires PLD1 to promote phagocytosis.

- A ARL11 expression is enriched in macrophages. Analysis of single-cell RNA-sequencing dataset shows that *ARL11* expression is highest in macrophages (<https://www.proteinatlas.org/ENSG00000152213-ARL11/tissue+cell+type>).
- B *ARL11* knockout of THP-1 stable cell pools. *ARL11* knockout THP-1 cell pools were generated by the CRISPR/Cas9 technology with three different-guide RNAs. Cell lysates were immunoblotted with the indicated antibodies.
- C *ARL11* knockout inhibits phagocytosis. Macrophages were differentiated from THP1 cell pools, followed by incubation with green zymosan particles for 1.5 h. Free green zymosan particles were washed away before photography. Details were described in Methods. Typically, all cells and cellular particles in randomly selected fields were counted. Data are presented as mean \pm SD, $n = 5$ technically independent samples. One-way ANOVA, $*P < 0.05$.
- D THP-1 cell pool stably expressing HA-tagged *ARL11*^{Q67L} or *ARL11*^{T26N}. Lysates were immunoblotted with indicated antibodies.
- E *ARL11*^{Q67L}, but not *ARL11*^{T26N}, promotes phagocytosis of macrophages. Macrophages were differentiated from indicated THP1 cell pool, followed by incubated with green zymosan particles for 1 h. Scale bars: 50 μ m. The result is representative of two biologically independent experiments.
- F Quantification result of (E). Data are presented as mean \pm SD, $n = 8$ technically independent samples. One-way ANOVA, $*P < 0.05$.
- G *PLD1* knockout efficiency and HA-tagged *ARL11*^{Q67L} expression of THP-1 stable cell pools. Lysates were immunoblotted with indicated antibodies.
- H *PLD1* knockout blocks the *ARL11*^{Q67L}-stimulated phagocytosis. Macrophages were differentiated from indicated THP1 cell groups and then incubated with green zymosan particles for 1.5 h. Scale bars: 50 μ m. The result is representative of two biologically independent experiments.
- I *PLD1* is required for *ARL11* to stimulate phagocytosis. Data are quantification of panel (H). Data are presented as mean \pm SD, $n = 5$ technically independent samples. Two-way ANOVA, $*P < 0.05$.

Source data are available online for this figure.

knockout of *ARL5A/5B* significantly decreased the colocalization of PI4KB with TGN46 (Fig 6E), but had little effect on the PI4KB colocalization with GM130 or Giantin (Appendix Fig S6C and D). We conclude that *ARL5A/5B* may specifically recruit PI4KB to the trans-Golgi network.

PI4KB is composed of an N-terminal non-catalytic helical region and a C-terminal kinase domain (Fig 6F; Burke, 2018). We generated various deletion constructs to map the domain in PI4KB responsible for *ARL5B* interaction. We found that a deletion of the N-terminal disordered region (N1), but not other domains, abolished *ARL5B* binding (Fig 6F and G). The N1 region of PI4KB was reported to interact with the Q domain of ACBD3, thereby required

for Golgi recruitment and promotion of PI4P synthesis on the Golgi membrane (Greninger et al, 2013). mEGFP-P4M-SidMx2 is a PI4P sensor widely used to detect cellular pools of PI4P (Hammond et al, 2014). We speculate that local PI4KB recruitment/activation may increase PI4P, thus increasing mEGFP-P4M-SidMx2 signals. Indeed, we found that both *ARL5A* and *ARL5B* showed strong colocalization with PI4P sensor mEGFP-P4M-SidMx2, particularly at the Golgi (Fig 6H). In contrast, ARF1 and RAB14 showed weaker colocalization with the PI4P sensor mEGFP-P4M-SidMx2, whereas RAB11A showed little colocalization (Appendix Fig S6E and F). In addition, *ARL5A*^{Q70L} showed stronger colocalization with the PI4P sensor than *ARL5A*^{WT}, while *ARL5A*^{T30N} showed even weaker

Figure 6. PI4KB is an ARL5A- and ARL5B-interacting protein.

- A PI4KB is enriched by *ARL5A* and *ARL5B*. *ARL5A*, *ARL5B*, and *RAB14* rank the top 3 GTPases based on PI4KB enrichment by miniTurbo screening of the GTP-bound forms of the Ras superfamily. For ARF family, data were from two biologically independent analyses, while for other GTPases, data were from one biological sample.
- B Interaction of PI4KB with *ARL5A/5B* is stronger than with ARF1, RAB11A/11B, and RAB14. Flag-tagged PI4KB was co-expressed with HA-tagged GTP-bound mutant of GTPases in HEK293A cells as indicated. PI4KB was immunoprecipitated with Flag beads, and the coprecipitated GTPases were detected by HA Western blot. The result is representative of three biologically independent experiments.
- C PI4KB preferentially binds to the GTP form of *ARL5B*. Flag-tagged PI4KB was co-expressed with HA-tagged *ARL5B*^{Q70L} (GTP-form) or *ARL5B*^{T30N} (GDP-form) mutant in HEK293A cells. Interaction was measured similar to panel B. The result is representative of two biologically independent experiments.
- D The *ARL5A* colocalization with PI4KB is GTP-dependent. HA-tagged GTP-bound *ARL5A*^{Q70L}, wild-type *ARL5A*, or GDP-bound *ARL5A*^{T30N} was co-expressed with Flag-tagged PI4KB. After 24 h, cells were fixed, followed by incubation with anti-Flag and anti-HA primary antibodies. DAPI (blue) was used for DNA staining. Scale bars: 10 μ m. Shown is representative of two biologically independent experiments. The left panel is the quantification of the overlap coefficient. Mean \pm SD, $n = 6$ technically independent samples. One-way ANOVA, $*P < 0.05$.
- E *ARL5A/5B* double knockout diminishes the colocalization of PI4KB and TGN46. Flag-tagged PI4KB was expressed in HEK293A wild-type or two *ARL5A/5B* double knockout clones as indicated. After 24 h, cells were fixed, followed by incubation with anti-Flag and anti-TGN46 primary antibodies. DAPI (blue) was used for DNA staining. Scale bars: 5 μ m. The result is representative of two biologically independent experiments. The left panel is the quantification of the overlap coefficient. Mean \pm SD, $n = 6$ technically independent samples. One-way ANOVA, $*P < 0.05$.
- F Schematic representation of the full-length PI4KB and various truncations. Δ N, deletion of the N-terminal region (1-306aa); Δ C, deletion of the C-terminal kinase domain (307-801aa); Δ N1, deletion of the N-terminal disordered region (1-127aa); Δ N2, deletion of the helical domain (128-242aa); and Δ N3, deletion of the helical-kinase linker region (243-306aa). "+" denotes positive interaction with *ARL5B*, and "-" denotes no interaction.
- G The N1 region of PI4KB is required for the interaction with *ARL5B*. Flag-tagged full-length or truncations of PI4KB were co-expressed with HA-tagged *ARL5B*^{Q70L}. PI4KB was immunoprecipitated with Flag beads, and the coprecipitated *ARL5B* was detected by HA Western blot. The result is representative of three biologically independent experiments.
- H The N1 region of PI4KB is required for the colocalization of *ARL5A/B* and PI4P. P4Mx2-mEGFP was co-expressed with HA-tagged *ARL5A*^{Q70L} in HEK293A wild-type or *PI4KB* knockout cells (clone#2-5). HEK293A cells were cotransfected with indicated constructs. After 24 h, cells were fixed with 4% paraformaldehyde, followed by incubation with anti-HA primary antibodies. DAPI (blue) was used for nucleus staining. Scale bars: 10 μ m. The result is representative of two biologically independent experiments.
- I Mander's overlap coefficient of (H). Mean \pm SD, $n = 8$ technically independent samples. One-way ANOVA, $*P < 0.05$.

Source data are available online for this figure.

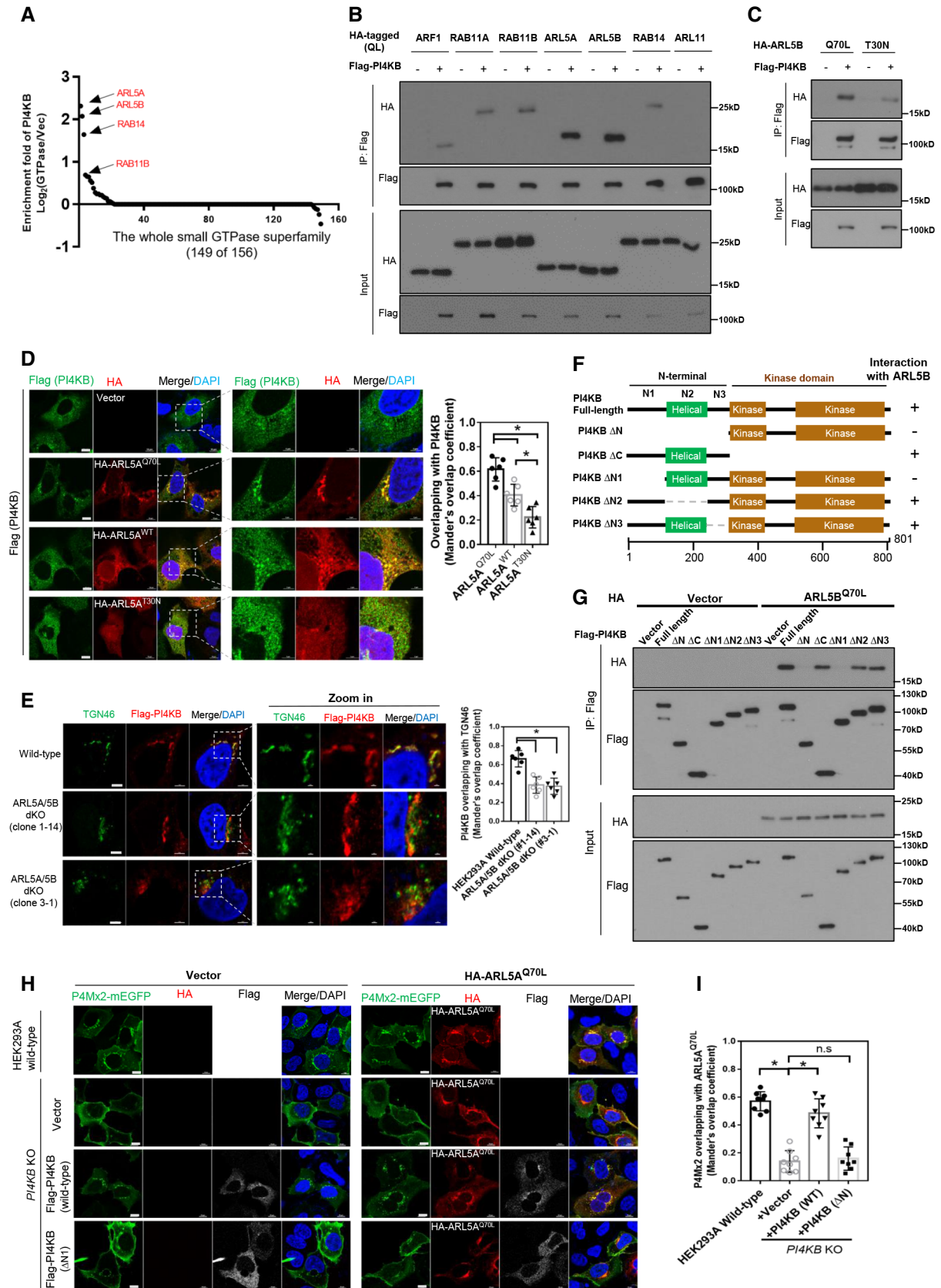


Figure 6.

colocalization with PI4P (Appendix Fig S6G and H), consistent with a notion that ARL5A and ARL5B recruit PI4KB in a GTP-dependent manner to increase local PI4P levels.

PI4P generation is controlled by four PI-4-kinases (PI4Ks) in mammals, namely PI4KA, PI4KB, PI4K2A, and PI4K2B (Balla & Balla, 2006; Burke, 2018). We performed co-immunoprecipitation experiments and observed that ARL5A and ARL5B specifically interacted with PI4KB, but not PI4KA, PI4K2A, and PI4K2B (Appendix Fig S6I). These observations are consistent with our finding that the ARL5A/5B fusion proteins exclusively labeled PI4KB, but not other PI4 kinases. We tested whether PI4KB is required for ARL5A and ARL5B to increase PI4P. To this end, *PI4KB* was deleted in HEK293A cells by CRISPR/Cas9; then, the effect of ARL5A and ARL5B on the PI4P sensor mEGFP-P4M-SidMx2 was determined. We observed that PI4KB knockout significantly diminished the colocalization of ARL5A/B with the PI4P sensor mEGFP-P4M-SidMx2 (Fig 6H and I). Notably, PI4KB knockout reduced PI4P at the Golgi complex, consistent with a prominent role of PI4KB there. Re-expression of wild-type PI4KB rescued the ARL5A colocalization with mEGFP-P4M-SidMx2. Moreover, the expression of the ARL5A binding-defective mutant PI4KB Δ N1 did not restore the colocalization of ARL5A and PI4P. These results are consistent with a model that interaction with PI4KB is important for ARL5A to increase PI4P. However, no PI4KB activation was seen using an *in vitro* lipid kinase assay (Appendix Fig S6J). Taken together, we propose that ARL5A/5B may recruit PI4KB to specific membrane domains to promote PI4P generation.

To determine the biological function of ARL5A/5B in stimulating PI4P synthesis, we first tested whether recruitment of ARL5A/5B to a specific membrane compartment could increase PI4P locally. Rapamycin efficiently induces the heterodimerization of the FK506 binding protein (FKBP) and the FKBP-rapamycin binding domain (FRB) (Fig 7A; Chen *et al*, 1995). Mitochondria have little PI4P, so they

were chosen as a surrogate target to investigate the role of ARL5A/5B in PI4KB-mediated PI4P synthesis by artificially targeting ARL5A/5B on mitochondria in a rapamycin-inducible manner. The FRB and FKBP domains were fused to a Tom20-derived mitochondrial targeting sequence and ARL5A/5B, respectively (Fig 7A; Miyamoto *et al*, 2021). The FKBP-RFP control or FKBP-RFP-ARL5A/5B fusion constructs were cotransfected with the FRB-Tom20 fusion into HEK293A cells. In the absence of rapamycin, cellular PI4P, detected by the P4Mx2 sensor, localized at the perinuclear region and plasma membrane, with little signal on the mitochondria (Hammond *et al*, 2014; Zewe *et al*, 2020) (Fig 7B). Upon rapamycin treatment, as expected both FKBP-RFP-ARL5A and FKBP-RFP-ARL5B were translocated to the mitochondria. Importantly, rapamycin induced mitochondrial PI4P in cells expressing FKBP-RFP-ARL5A or FKBP-RFP-ARL5B, but not the FKBP-RFP control (Fig 7D). In addition, upon rapamycin treatment the perinuclear PI4P signal was also reduced in the FKBP-RFP-ARL5A- or FKBP-RFP-ARL5B-transfected cells (Fig 7B), possibly due to depletion of PI4KB from Golgi by the mitochondrially localized FKBP-RFP-ARL5A/5B. These results indicate that ARL5A/5B can increase PI4P when recruited to membrane surfaces.

To determine the role of PI4KB in ARL5A/5B-regulated PI4P production, we performed the above rapamycin-induced mitochondrial targeting experiments in PI4KB knockout cells (Appendix Fig S7C). PI4KB knockout did not affect the mitochondrial translocation of FKBP-RFP-ARL5A or FKBP-RFP-ARL5B in response to rapamycin. However, the PI4KB knockout abolished the rapamycin-induced and ARL5A/5B-dependent mitochondrial PI4P accumulation (Fig 7C and D). In contrast, PI4KA knockout did not affect the ARL5A/5B-dependent PI4P accumulation on mitochondria (Appendix Fig S7A). Moreover, the knockout of PI4K2A and PI4K2B did not affect the ARL5A/5B-induced mitochondrial PI4P accumulation (Appendix Fig S7B and C). Together, our results support a model that ARL5A/5B function to selectively recruit PI4KB to produce PI4P locally.

Figure 7. ARL5A/5B promote PI4P generation and protein secretion dependent on PI4KB.

- A Schematic representation of the rapamycin-induced mitochondria translocation of ARL5A/5B. The FRB domain was fused with the Tom20-derived mitochondrial anchor sequence. ARL5A/5B were fused with RFP and FKBP. Rapamycin induces the dimer formation of FRB and FKBP, therefore recruiting the FKBP-RFP-ARL5A/5B to mitochondria.
- B ARL5A/5B recruitment to mitochondria induces PI4P accumulation at the mitochondria. Tom20-CFP-RFB and P4Mx2-mEGFP were co-expressed with RFP-FKBP vector or RFP-FKBP-ARL5A/5B^{Q70L} constructs in HEK293A cells. Cell samples were treated with or without 100 nM rapamycin for 1 h. Scale bars: 10 μ m. The dashed line box indicates the merged signal of PI4P with ARL5A/5B or Tom20. The result is representative of two biologically independent experiments.
- C *PI4KB* knockout blocks the PI4P accumulation induced by mitochondria-anchored ARL5A/5B. Tom20-CFP-RFB and P4Mx2-mEGFP were co-expressed with RFP-FKBP vector or RFP-FKBP-ARL5A/5B^{Q70L} constructs in HEK293A *PI4KB* knockout cells (clone#2–5). Cell samples were treated with or without 100 nM rapamycin for 1 h before imaging. Scale bars: 10 μ m. The dashed line box indicates the merged signal of PI4P with ARL5A/5B or Tom20. The result is representative of two biologically independent experiments.
- D Mander's overlap coefficient of (B and C, result of rapamycin treatment). Mean \pm SD, $n = 5$ technically independent samples. Two-way ANOVA, * $P < 0.05$.
- E ARL5A/5B double knockout decreases protein secretion. Gaussia luciferase was expressed in HEK293A wild-type or three ARL5A/5B double knockout clones as indicated. After 24 h, the medium was replaced with the fresh medium. After 4 h, the medium was collected, and the secreted Gaussia luciferase was detected by Western blot. Cells were also collected and probed with indicated antibodies.
- F ARL5A/5B double knockout decreases protein secretion. Experiments were similar to panel (E). The medium was collected at the indicated time points and measured for luciferase activity. The cellular firefly luciferase activity was measured as the transfection control. Details were described in the Methods part. 3 μ g/ml BFA was used as a positive control to inhibit protein secretion. Data are presented as mean \pm SD, $n = 3$ biologically independent samples. One-way ANOVA, * $P < 0.05$.
- G *PI4KB* knockout blocks protein secretion stimulated by ARL5A/5B^{Q70L}. Gaussia luciferase was co-expressed with HA-tagged ARL5A^{Q70L} or ARL5B^{Q70L} in HEK293A wild-type or two *PI4KB* knockout cell lines as indicated. After 24 h, the medium was replaced with the fresh medium. After 3 h, the medium was collected and measured for Gaussia luciferase activity. Data are presented as mean \pm SD, $n = 3$ biologically independent samples. Two-way ANOVA, n.s denotes not significant, * $P < 0.05$.
- H *PI4KB* knockout blocks protein secretion stimulated by ARL5A/5B^{Q70L}. Experiments were similar to panel (G). Gaussia luciferase in culture medium was detected by Western blot, and the cell lysate was immunoblotted with indicated antibodies.
- I A proposed model of PI4KB regulation by ARL5A/5B. In addition to the reported ARF1, ACBD3, and RAB11A/11B, ARL5A/5B act as novel regulators of PI4KB to promote PI4P synthesis and protein secretion.

Source data are available online for this figure.

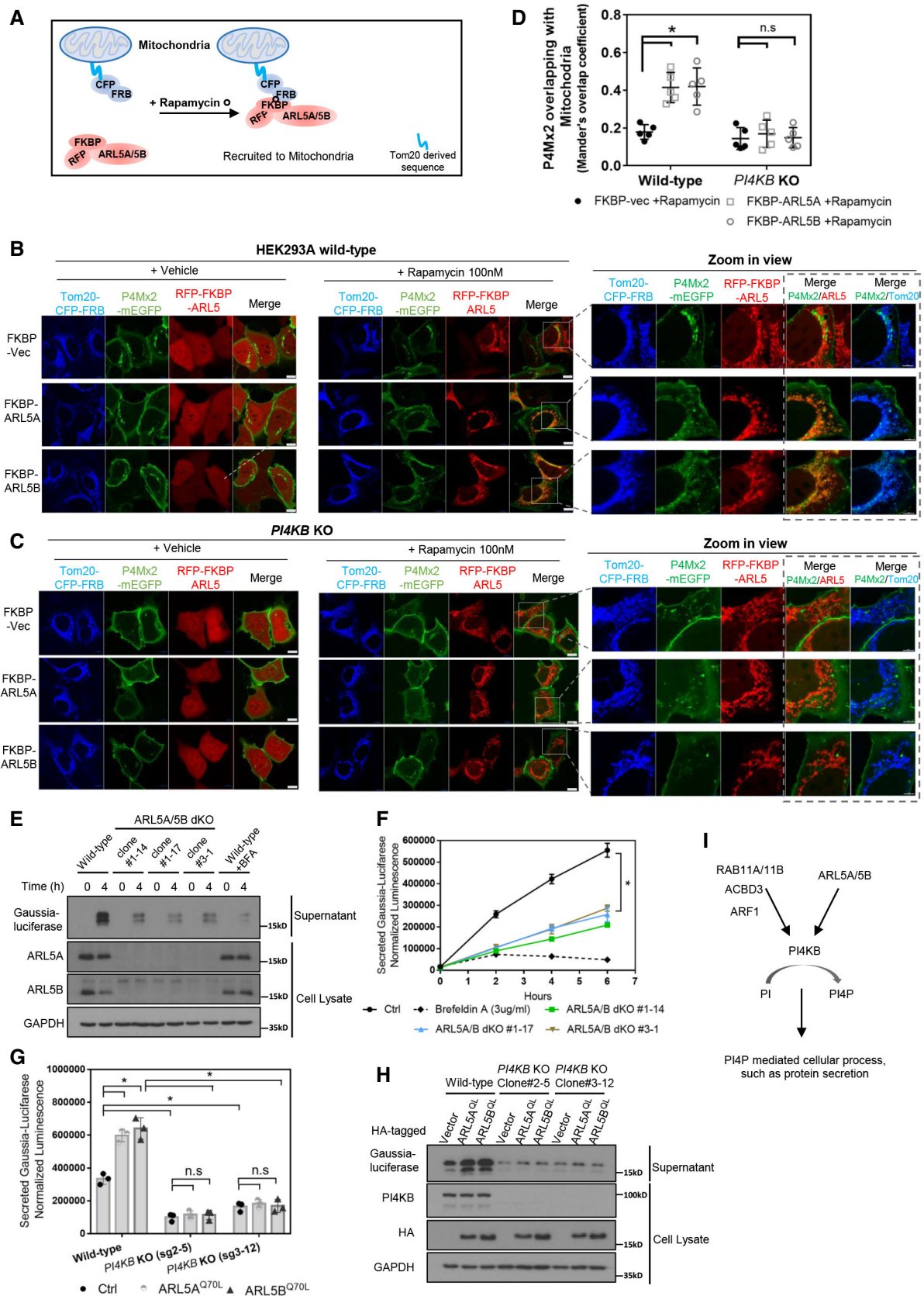


Figure 7.

ARL5A/5B promotes protein secretion via PI4KB

PI4KB-mediated PI4P synthesis at the Golgi complex has been reported to control vesicle biogenesis, membrane trafficking, and protein secretion (Boura & Nencka, 2015). We investigated the possible role of the ARL5A/5B-PI4KB connection in protein secretion. We generated three ARL5A and ARL5B double knockout (dKO) cell lines using the CRISPR/Cas9 technology (Fig 7E). Protein secretion was determined using the Gaussia luciferase secretion as a marker (Tannous, 2009). ARL5A and ARL5B double knockout reduced Gaussia luciferase secretion as determined by Western blot and luciferase assay of the cultured medium (Fig 7E and F). Consistent with the ARL5A/5B knockout experiments, the overexpression of the GTP forms of ARL5A/5B stimulated Gaussia luciferase secretion, while the GDP forms of ARL5A/5B failed to stimulate secretion (Appendix Fig S7D and E). Finally, we examined the role of PI4KB in ARL5A/5B-induced protein secretion. PI4KB knockout reduced the basal secretion of Gaussia luciferase. Importantly, PI4KB knockout completely blocked the stimulatory effect of ARL5A or ARL5B on protein secretion (Fig 7G and H). Taken together, the above data support a model in which ARL5A/5B act through PI4KB to promote protein secretion (Fig 7I).

Discussion

The Ras GTPase superfamily is involved in a wide range of physiological and pathological events. Ras GTPases initiate signal transduction through physical interaction with their downstream effectors. Compared with Ras and Rho families, the Arf subfamily is less studied. Using the miniTurboID-TMT-MS approach, we established an Arf GTPase interactome. To our knowledge, this study is the first report of applying miniTurboID coupled with a quantitative MS approach to systematically map the proximal interaction network of a particular protein family, allowing us to identify novel interactions in an unbiased manner. Our study not only confirmed well-established Arf-interacting proteins but also discovered a large number of new interactors. It should be noted that the miniTurbo is very sensitive and can label proteins in the close vicinity of the bait. Therefore, many proteins enriched in our interactome might not be physically interacting with the Arf family GTPases. They could be components in complex with a direct GTPase interactor or that share the same fine localization. It should be noted that the miniTurboID fusion may induce stereo-hindrance on protein–protein interaction. Another caveat is that overexpressed protein may not behave the same as the endogenous counterpart. Moreover, our approach cannot capture all protein–protein interaction, especially those occur under certain culture conditions, such as ARL3 interaction proteins in cilium that is induced by certain culture conditions. Nevertheless, the unbiased interactome provides valuable leads for future studies. Indeed, this study reveals previously unknown regulation of PLD1 and PI4KB by ARL11/14 and ARL5A/5B, respectively.

The function of PLD1 in cellular regulation has been extensively studied. It has been long recognized that GTP γ S-incubated cell lysate contains activation factors for PLD1 and the Arf family members, but neither ARL11 nor ARL14 were implicated in PLD1 activation (Bocckino et al, 1987; Brown et al, 1993; Cockcroft et al, 1994). The earlier studies were largely done by *in vitro* assays

focusing on the classic Arf members. Based on the unbiased screening here, our study reveals a novel interaction of PLD1 with ARL11 and ARL14. Furthermore, PLD1 shows stronger interaction with and activation by ARL11 and ARL14 compared with ARF1, ARF6, and RHOA, suggesting that ARL11 and ARL14 are important physiological regulators of PLD1. This model does not exclude that PLD1 may also be regulated by the other GTPases. We further speculate that different GTPases may regulate PLD1 at different subcellular compartments in response to different upstream signals and in different cell types. In addition, different GTPases may regulate PLD1 via different mechanisms. For example, RHOA was reported to bind the C-terminal region of PLD1 protein, as opposed to the loop region by ARL11 and ARL14 (Yamazaki et al, 1999). Further, our study uncovered a new function of ARL11 in promoting phagocytosis in macrophage-like cells and this function of ARL11 is dependent on PLD1. ARL14 expression is highly restricted in enterocytes, panel cells, and gastric mucus-secreting cells (Appendix Fig S5B). Future studies are needed to determine whether ARL14 may play a role in secretion and the role of PLD1.

Previous studies have shown that only PLD1, but not PLD2, could be activated by the Arf family GTPases (Massenburg et al, 1994; Hammond et al, 1997; Exton, 2000). However, the reason for this selective regulation of PLD1 versus PLD2 is unknown. Our domain mapping experiment revealed that the loop region of PLD1 mediates the binding and activation by ARL11 and ARL14. Interestingly, this loop region, predicted to be intrinsically disordered, is unique to PLD1. The loop region has been reported to mediate the inhibition of PLD1 or serve as an effector regulatory region (Sung et al, 1999), while the mechanism is unknown. The loop region-dependent PLD1 activation by ARL11 and ARL14 provides a possible explanation for the differential modulation of PLD1 and PLD2 (Frohman, 2015).

PI4KB does not contain a specific localization signal and can be recruited to the cellular membrane mainly via protein–protein interactions, such as through the small GTPase Arf1 or the Golgi adaptor protein ACBD3, which is necessary for generating a PI4P-enriched microenvironment on Golgi (Boura & Nencka, 2015). However, it has been reported that Arf1 and ACBD3 are dispensable for PI4KB recruitment to the Golgi in certain contexts (Dorobantu et al, 2014; Dorobantu et al, 2015), suggesting that there are unknown factors mediating the recruitment. Besides the GARP complex, few downstream effectors of ARL5A and ARL5B are known (Rosa-Ferreira et al, 2015). Consistent with a functional relationship between PI4KB and ARL5A/5B, artificial targeting of ARL5A or ARL5B to mitochondria increased PI4P on mitochondria in a manner dependent on PI4KB. We further propose that ARL5A and ARL5B promote protein secretion via PI4KB. Targeting PI4KB has emerged as a promising strategy to inhibit the intracellular development of malarial pathogens, or the replication of a wide range of RNA viruses (Hsu et al, 2010; Sasaki et al, 2012). The ARL5A/ARL5B and PI4KB connection may provide potential targets for antiviral or malarial therapy.

Materials and Methods

Antibodies

Antibodies against Vinculin (V9131) and FLAG-HRP (A8592) were purchased from MilliporeSigma. Antibodies against FLAG-tag

(#14793), HA-tag (#3724), HA-HRP (#2999), and PLD1 (#3832) were purchased from Cell Signaling Technology. Antibodies against GAPDH (47724), ARF1 (sc-53168), ARF6 (sc-7971), ARL5A (sc-514680), and ARL5B (sc-393511) were purchased from Santa Cruz Biotechnology. Antibody against ARL11 (NBP2-01470) was purchased from Novus Biologicals. Antibodies against PI4KA (12411-1-AP), PI4KB (13247-1-AP), PI4K2A (15318-1-AP), and PI4K2B (15074-1-AP) were purchased from Proteintech. Antibody against Gaussia luciferase (PA1-181) was purchased from Thermo Fisher Scientific.

Plasmids

cDNAs of Ras superfamily GTPases were obtained by RT-PCR of mRNA from several human cell lines. GTPase cDNAs were verified by Sanger DNA sequencing. GTP-bound mutant of ARF fused with miniTurbo was cloned into the pCDH-EF1a-MCS vector. Full-length or truncated cDNA of human PLD1 and PI4KB was cloned into the pRK7-N-FLAG vector using standard protocols. The cDNA of human ARF1, ARF6, ARL11, ARL14, ARL5A, and ARL5B was cloned into the pRK7-C-HA vector. The cDNA of wild-type or indicated mutant of RAB11A, RAB11B, and RHOA was cloned into the pRK7-N-HA vector. Full length of PLD1 or ARL11 was cloned into the pCDH-EF1a-MCS vector. Tom20-CFP-FRB plasmid was a kind gift from Takafumi Miyamoto (Addgene plasmid # 171461). The plasmids px459 vector and lenti-CRISPR v2 were provided by Dr. Feng Zhang (Addgene plasmid #62988 & #52961). The plasmids pCMV-GLuc and pCMV-FLuc were purchased from Thermo Scientific™ (#16147 and #16156). Point mutations were generated by standard mutagenesis kit Q5® High-Fidelity DNA Polymerase (NEB #M0491). All constructions were confirmed by DNA sequencing before further applications.

Chemicals

Biotin, sodium dodecyl sulfate, Nonidet P-40 Substitute, GTP γ S, dithiothreitol, Iodoacetamide, and urea were purchased from Sigma-Aldrich. Lipofectamine 3000, streptavidin-coated magnetic beads, Protein A/G Magnetic Beads, Tandem Mass Tag Reagent, 4',6-diamidino-2-phenylindole, dihydrochloride (DAPI), and trifluoroacetic acid were purchased from Thermo Fisher Scientific. Puromycin and fetal bovine serum were purchased from Gibco. Brefeldin A was purchased from BioLegend (420601). Rapamycin was purchased from Selleck Chemical (S1039).

MiniTurboID

Proximal proteins of ARF GTPase were biotinylated and isolated using the TurboID methods (Branon *et al*, 2018) with a few modifications. Briefly, HEK293A cells were infected with lentivirus expressing ARF-miniTurbo fusion protein or Vector-miniTurbo as a control, and stable cell pools were selected. The medium was supplemented with 1 μ M biotin for 15 min before harvest. Cells were washed 3 times on ice-cold phosphate-buffered saline (PBS) and lysed in RIPA lysis buffer (150 mM NaCl, 50 mM Tris [pH 7.5], 1% NP-40, 0.5% sodium deoxycholate, and 0.1% SDS). Affinity purification was done with streptavidin-coated magnetic beads (Thermo Fisher #88817, 20 μ l of slurry per 100-mm dish cells). Protein

samples on magnetic beads were subsequently washed twice with 1 ml of RIPA lysis buffer, once with 1 ml of 1% SDS, once with 1 ml of 1 M KCl, once with 1 ml of 0.1 M Na₂CO₃, and twice with 1 ml of 2 M urea in 50 mM Tris-HCl (pH 7.4). These beads were incubated with 200 μ l of 2 M urea/50 mM Tris containing 1 mM DTT and 0.6 μ g sequencing-grade trypsin (Promega, #V5111) for 1 h at 37°C with shaking. After 1 h, the eluate was reduced in 3.3 mM DTT for 30 min at 25°C with shaking. The samples were alkylated with 10 mM iodoacetamide at 25°C with shaking and protected from light. After 40 min, an additional 0.4 μ g of trypsin was added to the sample and the digestion was completed overnight at 37°C with shaking. Digested samples were acidified using trifluoroacetic acid (TFA) to a final concentration of 0.5%. Peptide samples were desalted on C18 Sep-Pak cartridges (Waters) and evaporated to dryness in a vacuum concentrator.

Tandem mass tag (TMT) labeling and hydrophilic interaction liquid chromatography (HILIC) fractionation

Each peptide sample was resuspended in 25 mM phosphate buffer (pH8.0) and labeled with one isobaric TMT reagent (Thermo Scientific, #90110) overnight at room temperature. Five samples, each labeled with a different TMT, were combined and desalted with C18 columns and dried under speed-vac. The combined peptide samples were fractionated using a Thermo Fisher Dionex UltiMate 3000 HPG-3400 M pump and WPS3000T autosampler, operated under Chromeleon v7.2. 100% acetonitrile and 2% trifluoroacetic acid served as buffer A and B for the mobile phase of the run, respectively. Peptides were resuspended in 100 μ l UHP diH₂O and loaded onto a TSKgel-Amide-80 column (5 μ m particle size, 1 mm ID, 15 cm, #0021486) at room temperature at a flow rate of 40 μ l/min. The peptides were fractionated with the following gradient: 0–24 min at 10% B, 24–31 min from 10 to 19% B, 31–55 min from 19 to 32% B, 55–59 min from 32 to 95% B, 59–68 min at 95% B, 68–72 min from 95 to 10% B, and 72–90 min at 10% B. Fourteen fractions were collected between 37 and 74 min of the gradient, dried via speed-vac, and combined into 5 samples to then be analyzed by LC-MS.

LC-MS

Data acquisition was performed on a Thermo Fisher Scientific Orbitrap Fusion Lumos mass spectrometer coupled to a Thermo Fisher Dionex UltiMate 3000 RSLCnano pump/RS Autosampler, operated under Xcalibur 4.2 and Tune 3.1. Peptides were resuspended in 5 μ l UHP diH₂O, and 1–2 μ l of the sample was loaded onto an in-house-packed column (Polymicro Technologies, 100 μ m, ID, #2000023) with 1 cm of C4 (Sepax 5 μ m, 120A, #109045-0000) and 12 cm of C18 (Sepax 2.2 μ m, 120A, #101182-0000). 100% acetonitrile + 0.1% formic acid and 0.1% formic acid were used for mobile phases A and B, respectively. The sample was eluted at a flow rate of 0.3 μ l/min at room temperature from 10% B to 35% B for 62 min, 35% to 80% B for 10 min, and 80% B for 10 min. For the mass spectrometer, the following settings were used: MS1 scan resolution, 120,000; range, between 375 and 1,400 m/z; AGC target, 5.0 \times 10⁵; maximum injection time, 100 ms; and time between master scans, 2 s. The 10 most abundant precursors with charge states 2–5 were selected for CID. The MS2 quadrupole isolation window

was set to 0.7 m/z, collision energy was set to 35% with 10-ms activation time and 3.0×10^4 minimum AGC target, and scan rate was set to rapid with 35-ms maximum injection time. Isobaric tag loss exclusion was enabled for TMT, and MS3 scan was set with MS1 isolation window of 1.2 m/z and MS2 isolation window of 3 m/z. MS3 was activated by HCD with 55% collision energy, detected with Orbitrap resolution of 30,000. Fragment ion scans between 125 and 135 m/z were recorded, with minimum AGC 5.0×10^4 and 100-ms maximum injection time. Dynamic exclusion duration was set to 30 s; after a single count, isotopes were excluded.

MS data analysis

Raw data were processed using Trans-Proteomic Pipeline (TPP), and peptides were analyzed via COMET peptide search engine. COMET search was performed against database UniProt 9606 UP5640 with the following general parameters: peptide mass tolerance of 20 ppm with monoisotopic parent masses, isotope error offset setting of 2, lysine and asparagine variable modification of 229.162932 with -1 term distance and maximum of 3 or 1 modifications per peptide, respectively, 1.0005 tolerance for ion trap MS/MS with 0.4 offset, and 0.02 tolerance for high-res MS/MS with 0.0 offset, and static modifications were made to cysteine, 57.021464, and methionine, 15.9949. Peptides were analyzed with Libra and checked against decoy hits, and the results of the output file below Peptide Prophet probability of 0.7 and the peptide length of 7 were filtered out. A TSV file was generated from results containing data above the minimum probability of 0.95 and minimum number of 2 peptides that satisfy the Libra criteria, before being processed in Excel. The normalized ratios of GTPase channel against the control channel were log₂-transformed. Data were normalized by subtracting the median to center the distribution at zero.

Bioinformatic analysis

Gene ontology (GO) categories of proximal proteins were generated using g:Profiler (Raudvere et al, 2019) to provide the GO terms (biological process), and then grouped by Revigo (Supek et al, 2011). Heatmap analysis was performed using R (www.r-project.org), and plotted with the Pheatmap without clustering or ComplexHeatmap package (Gu et al, 2016).

In vitro PLD1 activity assay

PLD1 activity was measured by assaying the release of ³H-choline from radiolabeled PC (American Radiolabeled Chemicals) within Triton X-100 mixed micelles. Details were described previously (Bowling et al, 2020). Briefly, the recombinant PLD1 and constitutively active form of GTPases were diluted in 20 mM Tris, 150 mM NaCl, pH 7.5. The small GTPases were activated after being EDTA-stripped and preloaded with GTPγS as described previously (Hammond et al, 1997). 50 μl of activated GTPase was mixed with 50 μl of purified PLD1 protein in a 10:1 GTPase:PLD1 molar ratio. Unstimulated samples were purified PLD1 mixed with buffer including 5 μM EDTA, 10 μM MgCl₂, and 1 μM GTPγS. A 25 μl of the protein mixture and 25 μl of mixed micelles were mixed and incubated at 37°C for 30 min and then quenched with a 2:1 chloroform:methanol solution. After vortexing and centrifugation, the aqueous layer,

which contained the ³H-choline released product, was extracted and CPMs were quantitated using a scintillation counter. All reactions were linear with respect to PLD1 concentration and time.

Phagocytosis assay

Phagocytosis activity was measured by assaying the uptake of green Zymosan prepared from cell wall of *Saccharomyces cerevisiae* (BioVision, K397). Briefly, THP-1-derived macrophages were seeded overnight at 2×10^5 of viable cells in the glass-bottom dishes (MatTek, P35G-1.5-10-C). The next day, the cells were incubated with 6 μl of Zymosan particles for 1.5 h, followed by washing with PBS for 4 times. The amount of engulfed Zymosan was recorded by fluorescence microscope and counted. A 5–10 random fields were chosen for each group. Typically, each field contains 50–100 cells.

PI4KB kinase activity assay

PI4KB kinase activity was measured by assaying the release of ADP using the ADP-Glo assay. Details were described in Tai et al (2011) with some modifications. Briefly, the recombinant PI4KB (PV5277, Thermo Fisher) was diluted in kinase buffer (40 mM Tris-HCl, pH 7.5, 20 mM MgCl₂, 1 mM EGTA, 0.2% Triton X-100). The small GTP-binding proteins were activated after being EDTA-stripped and preloaded with GTPγS. The lipid substrates are small unilamellar vesicles containing a mixture of phosphatidylinositol (PI) at a 1:3 ratio with phosphatidylserine (PS) as carrier lipid (V1711, Promega). For each kinase reaction, activated GTPase mixed with PI4KB protein in a 20:1 ratio was added to 10 μl of 2.5X kinase Reaction Buffer and 10 μl 2.5X Lipid Substrate working solution. The final concentration of PI4KB protein is 10 nM. 5 μl of 125 μM ATP was added to start the reaction, followed by incubating for 1 h at 23°C. Blanks were determined using buffer in place of enzyme. The release of ADP was measured by the ADP-Glo assay (V6930, Promega). The luminescence intensity was determined with the plate-reading luminometer (Infinite 200Pro, Tecan).

Secretion assay

Protein secretion activity was measured by assaying the secretion of a *Gaussia* luciferase into the culture medium. Briefly, indicated HEK293A cells were cotransfected with pCMV-GLuc and pCMV-FLuc with Lipofectamine 3000 (Invitrogen) in 96-well plates. The next day, the medium was changed to 100 μl fresh medium. 3 μg/ml BFA was used as a positive control for inhibition of protein secretion. After incubation, the medium was collected, followed by measuring the *Gaussia* luciferase activity with the *Gaussia* luciferase Glow assay kit (16160, Pierce™) or measuring the *Gaussia* luciferase protein abundance with *Gaussia* luciferase antibody using Western blot. Firefly luciferase activity was measured according to the manufacturer's protocol (16176, Pierce™) as an internal control.

Cell culture and transfection

All cell lines were maintained at 37° with 5% CO₂. HEK293A cells were purchased from Thermo Fisher (Cat#R70507) and cultured in Dulbecco's modified Eagle's medium (GIBCO). THP-1 cells were purchased from ATCC (Cat#TIB-202) and cultured in RPMI-1640

medium (Invitrogen). All the above media were supplemented with 10% fetal bovine serum (FBS) (Gibco) and 50 µg/ml penicillin/streptomycin. These cell lines were negative when the mycoplasma contamination test was performed. Plasmid transfection was carried out using PolyJet DNA *In Vitro* Transfection Reagent (SignaGen, SL100688) or Lipofectamine 3000 (Invitrogen, L3000).

Immunoprecipitation and Western blotting

Cells were lysed in ice-cold NP-40 buffer containing 50 mM Tris-HCl (pH 7.5), 150 mM NaCl, 0.3% NP-40 with protease inhibitors (Roche, #11873580001), and 1 mM PMSF. Cell lysate was centrifuged at 12,000 *g* for 15 min at 4°C. The supernatant was incubated with Flag beads (Sigma) for 3 h at 4°C, or with indicated antibody for 2 h followed by incubation with Protein A/G Magnetic Beads (Thermo Scientific, 88803) for another 2 h at 4°C. After washing three times with ice-cold 0.1% NP-40 buffer, the proteins were denatured by SDS loading buffer containing DTT for further analysis.

Generation of knockout cells using CRISPR/Cas9 technique

The gene deletion used in this study was carried out by the CRISPR/Cas9-mediated gene-editing system. The single-guide RNA (sgRNA) sequences were designed using the ChopChop tool (<https://chopchop.cbu.uib.no/>). Two or three sgRNA sequences targeting the human *ARL11*, *PLD1*, *ARL5A*, *ARL5B*, or *PI4KB* gene deletion were used. Gene deletion was verified by Sanger sequencing of genomic DNA or Western blotting of cell lysates. The guide sequences targeting the human *ARL11*, *PLD1*, *ARL5A*, *ARL5B*, *PI4KA*, *PI4KB*, *PI4K2A*, and *PI4K2B* genes were shown below:

ARL11 #1: 5'-TGAAGCCCGTTACCCGAGT-3'; *ARL11* #2: 5'-CAGCCGCCGACTCGGTAAG-3'; *ARL11* #3: 5'-CACGCTCCTTACAAGCTGA-3'; *PLD1* #1: 5'-GCGTCTACATCCCAACATAA-3'; *PLD1* #2: 5'-AGTGCAGAGGTATTTACCCG-3'; *ARL5A* #1: 5'-CACTTACTATATAACACAG-3'; *ARL5A* #3: 5'-TAATACACGTTTCTTAATGT-3'; *ARL5B* #1: 5'-GGTGATCTTCGCCAACTG-3'; *ARL5B* #3: 5'-CCGCCCGGTGCTCGTGATG-3'; *PI4KB* #2: 5'-TACTCCGAATTCGGTTCTCG-3'; *PI4KB* #3: 5'-CAATTGGGGAGATGGCCGTA-3'; *PI4KA* #1: 5'-CGCCGACGTTACCTTCTCCA-3'; *PI4K2A* #2: 5'-GAACTCGTTCCGCTCGCGGT-3'; *PI4K2B* #3: 5'-GGTTCGCACCTGAAACCGCG-3'.

Virus infection and exogenous gene expression

To generate THP-1 *ARL11* or *PLD1* knockout cell pool, lentiviruses carrying pLenti-V2 vector or pLenti-V2-guideRNA were produced in HEK293T cells using second-generation lentiviral system with packaging plasmids psPAX2, pMD2.g, and a lentiviral transfer vector at a ratio of 3:1:4. Viral supernatant was harvested 36 h after initial plasmid transfection, filtered through 0.45-µm filter, and mixed with polybrene (5 µg/ml) to increase the infection efficiency. Stable cell pools were selected with 1 µg/ml puromycin (Amresco) for 3 days.

To generate THP-1 cell pool stably expressing Q67L or T26N mutant of *ARL11*, lentiviruses carrying pCDH-EF1a-Vector or pCDH-EF1a-*ARL11*-HA were produced in HEK293T cells using psPAX2 and pMD2.g as packaging plasmids. Virus supernatant was filtered through 0.45-µm filter and used to infect THP-1 cells in the presence of 5 µg/ml polybrene.

Immunofluorescence staining

Cells seeded in glass-bottom dishes (MatTek, P35G-1.5-10-C) were washed with PBS two times for 1 min, fixed immediately with 4% paraformaldehyde for 15 min, and then permeabilized with 0.1% Triton X-100 in PBS for 10 min. After blocking in 3% BSA for 40 min, cells were incubated with primary antibodies overnight at 4°C. Cells were washed with PBS 3 times for 5 min, and Alexa Fluor-conjugated secondary antibodies were added for 1 h at room temperature. DAPI was used to stain DNA. Images were captured by a Nikon Eclipse Ti confocal microscope and then were exported from the NIS-Elements imaging software. Colocalization was quantified using Mander's overlap coefficient, which was calculated using the JACoP plug-in in ImageJ (Bolte & Cordelieres, 2006).

Experimental study design and statistical analysis

The sample size was determined based on the literature that tested the same cell lines or performed the similar assays, as well as recommended best practices in the field. There is no bias when collecting data. All the samples were randomly allocated into experimental groups. No predetermined sample size calculation was performed. The investigators were blinded during mass spectrometry experiment. The other experiments of this study were not done blinded. The samples' harvest process made it impossible to be blinded. No data were excluded from the experiment. Results were analyzed and graphed using the Prism 7.0 software (GraphPad Software). The *P*-value for the detection of significant outlier ratio is $\text{Significance} = \frac{1}{2} \operatorname{erfc}\left(\frac{z}{\sqrt{2}}\right) = \frac{1}{\sqrt{2\pi}} \int_z^{\infty} e^{-t^2/2} dt$, and adjusted with the Benjamini-Hochberg FDR threshold of 0.05 for multiple testing, which is performed by the Perseus software. Details were described in the reference (Cox & Mann, 2008). Data from biological or technical replicates are shown with standard deviation (mean ± SD). Statistical analyses were performed using two-tailed Student's *t*-test, and one-way or two-way analysis of variance (ANOVA) as indicated in corresponding figure legends. *P* < 0.05 was considered statistically significant.

Data availability

The full list of ARF-miniTurboID-TMT data in this manuscript can be found in the [Datasets EV1–EV25](#). All MS raw data have been deposited to the PRIDE database, which are available via ProteomeXchange with identifier PXD033382 (<http://proteomecentral.proteomexchange.org/cgi/GetDataset?ID=PXD033382>).

Expanded View for this article is available online.

Acknowledgements

We thank Guan laboratory members for intellectual input. This work was supported by research grants from the NIH GM51586, CA217642, and CA268179 to K.L.G. This work was supported by research grants from the NIH GM116897 and OD023498 to H.Z., J.M.F. is supported by NIH grant T32CA009523.

Author contributions

Fu-Long Li: Conceptualization; data curation; formal analysis; funding acquisition; validation; investigation; visualization; methodology; writing – original

draft; writing – review and editing. **Zhengming Wu:** Data curation; software; formal analysis; methodology. **Yong-Qi Gao:** Data curation; software; formal analysis; methodology. **Forrest Z Bowling:** Data curation; formal analysis; methodology. **J Matthew Franklin:** Software; methodology. **Chongze Hu:** Software; methodology. **Raymond T Suhandynata:** Data curation; methodology. **Michael A Frohman:** Formal analysis; methodology; writing – review and editing. **Michael V Airola:** Formal analysis; writing – review and editing. **Huilin Zhou:** Resources; formal analysis; funding acquisition; methodology; writing – review and editing. **Kun-Liang Guan:** Conceptualization; resources; formal analysis; supervision; funding acquisition; validation; investigation; methodology; writing – original draft; project administration; writing – review and editing.

In addition to the CRediT author contributions listed above, the contributions in detail are:

F-LL and K-LG conceived the project and wrote the manuscript. F-LL prepared the miniTurboID samples and performed most experiments in this study. ZW and CH performed the bioinformatics analyses. Y-QG and RTS performed the mass spectrometry analyses. FZB, performed the ARF-stimulated PLD1 activity assay. JMF assisted in the microscope experiments. MAF, MVA, and HZ assisted in experimental design and data analyses.

Disclosure and competing interests statement

K.-L.G. is a cofounder of and has an equity interest in Vivace Therapeutics. The other authors declare that they have no conflict of interest.

References

- Ali WH, Chen Q, Delgiorno KE, Su W, Hall JC, Hongu T, Tian H, Kanaho Y, Di Paolo G, Crawford HC *et al* (2013) Deficiencies of the lipid-signaling enzymes phospholipase D1 and D2 alter cytoskeletal organization, macrophage phagocytosis, and cytokine-stimulated neutrophil recruitment. *PLoS One* 8: e55325
- Antonicka H, Lin ZY, Janer A, Aaltonen MJ, Weraarpachai W, Gingras AC, Shoubridge EA (2020) A high-density human mitochondrial proximity interaction network. *Cell Metab* 32: 479–497.e479
- Arakel EC, Schwappach B (2018) Formation of COPI-coated vesicles at a glance. *J Cell Sci* 131: jcs209890
- Bagci H, Sriskandarajah N, Robert A, Boulais J, Elkholi IE, Tran V, Lin ZY, Thibault MP, Dube N, Faubert D *et al* (2020) Mapping the proximity interaction network of the rho-family GTPases reveals signalling pathways and regulatory mechanisms. *Nat Cell Biol* 22: 120–134
- Balla A, Balla T (2006) Phosphatidylinositol 4-kinases: old enzymes with emerging functions. *Trends Cell Biol* 16: 351–361
- Barlowe C, Orci L, Yeung T, Hosobuchi M, Hamamoto S, Salama N, Rexach MF, Ravazzola M, Amherdt M, Schekman R (1994) COPII: a membrane coat formed by sec proteins that drive vesicle budding from the endoplasmic reticulum. *Cell* 77: 895–907
- Belov GA, Habbersett C, Franco D, Ehrenfeld E (2007) Activation of cellular Arf GTPases by poliovirus protein 3CD correlates with virus replication. *J Virol* 81: 9259–9267
- Bocckino SB, Blackmore PF, Wilson PB, Exton JH (1987) Phosphatidate accumulation in hormone-treated hepatocytes via a phospholipase D mechanism. *J Biol Chem* 262: 15309–15315
- Bolte S, Cordelieres FP (2006) A guided tour into subcellular colocalization analysis in light microscopy. *J Microsc* 224: 213–232
- Boura E, Nencka R (2015) Phosphatidylinositol 4-kinases: function, structure, and inhibition. *Exp Cell Res* 337: 136–145
- Bowling FZ, Salazar CM, Bell JA, Huq TS, Frohman MA, Airola MV (2020) Crystal structure of human PLD1 provides insight into activation by PI(4,5)P2 and RhoA. *Nat Chem Biol* 16: 400–407
- Branon TC, Bosch JA, Sanchez AD, Udeshi ND, Svinikina T, Carr SA, Feldman JL, Perrimon N, Ting AY (2018) Efficient proximity labeling in living cells and organisms with TurboID. *Nat Biotechnol* 36: 880–887
- Brown HA, Gutowski S, Moomaw CR, Slaughter C, Sternweis PC (1993) ADP-ribosylation factor, a small GTP-dependent regulatory protein, stimulates phospholipase D activity. *Cell* 75: 1137–1144
- Burke JE (2018) Structural basis for regulation of phosphoinositide kinases and their involvement in human disease. *Mol Cell* 71: 653–673
- Calin GA, Trapasso F, Shimizu M, Dumitru CD, Yendamuri S, Godwin AK, Ferracin M, Bernardi G, Chatterjee D, Baldassarre G *et al* (2005) Familial cancer associated with a polymorphism in ARLTS1. *N Engl J Med* 352: 1667–1676
- Casalou C, Ferreira A, Barral DC (2020) The role of ARF family proteins and their regulators and effectors in cancer progression: a therapeutic perspective. *Front Cell Dev Biol* 8: 217
- Chen J, Zheng XF, Brown EJ, Schreiber SL (1995) Identification of an 11-kDa FKBP12-rapamycin-binding domain within the 289-kDa FKBP12-rapamycin-associated protein and characterization of a critical serine residue. *Proc Natl Acad Sci U S A* 92: 4947–4951
- Choi CR, Rhee HW (2022) Proximity labeling: an enzymatic tool for spatial biology. *Trends Biotechnol* 40: 145–148
- Cockcroft S, Thomas GM, Fensome A, Geny B, Cunningham E, Gout I, Hiles I, Totty NF, Truong O, Hsuan JJ (1994) Phospholipase D: a downstream effector of ARF in granulocytes. *Science* 263: 523–526
- Corrotte M, Chasserot-Golaz S, Huang P, Du G, Ktistakis NT, Frohman MA, Vitale N, Bader MF, Grant NJ (2006) Dynamics and function of phospholipase D and phosphatidic acid during phagocytosis. *Traffic* 7: 365–377
- Couzens AL, Knight JD, Kean MJ, Teo G, Weiss A, Dunham WH, Lin ZY, Bagshaw RD, Sicheri F, Pawson T *et al* (2013) Protein interaction network of the mammalian hippo pathway reveals mechanisms of kinase-phosphatase interactions. *Sci Signal* 6: rs15
- Cox J, Mann M (2008) MaxQuant enables high peptide identification rates, individualized p.p.b.-range mass accuracies and proteome-wide protein quantification. *Nat Biotechnol* 26: 1367–1372
- Donaldson JG, Jackson CL (2011) ARF family G proteins and their regulators: Roles in membrane transport, development and disease. *Nat Rev Mol Cell Biol* 12: 362–375
- Dorobantu CM, van der Schaar HM, Ford LA, Strating JR, Ulferts R, Fang Y, Belov G, van Kuppeveld FJ (2014) Recruitment of PI4KIIIbeta to coxsackievirus B3 replication organelles is independent of ACBD3, GBF1, and Arf1. *J Virol* 88: 2725–2736
- Dorobantu CM, Ford-Siltz LA, Sittig SP, Lanke KH, Belov GA, van Kuppeveld FJ, van der Schaar HM (2015) GBF1- and ACBD3-independent recruitment of PI4KIIIbeta to replication sites by rhinovirus 3A proteins. *J Virol* 89: 1913–1918
- Duden R (2003) ER-to-Golgi transport: COP I and COP II function (review). *Mol Membr Biol* 20: 197–207
- Exton JH (2000) Phospholipase D. *Ann N Y Acad Sci* 905: 61–68
- Frohman MA (2015) The phospholipase D superfamily as therapeutic targets. *Trends Pharmacol Sci* 36: 137–144
- Gillingham AK, Munro S (2007) The small G proteins of the Arf family and their regulators. *Annu Rev Cell Dev Biol* 23: 579–611
- Go CD, Knight JDR, Rajasekharan A, Rathod B, Hesketh GG, Abe KT, Youn JY, Samavarchi-Tehrani P, Zhang H, Zhu LY *et al* (2021) A proximity-dependent biotinylation map of a human cell. *Nature* 595: 120–124

- Godi A, Pertile P, Meyers R, Marra P, Di Tullio G, Iurisci C, Luini A, Corda D, De Matteis MA (1999) ARF mediates recruitment of PtdIns-4-OH kinase-beta and stimulates synthesis of PtdIns(4,5)P2 on the Golgi complex. *Nat Cell Biol* 1: 280–287
- de Graaf P, Zwart WT, van Dijken RA, Deneka M, Schulz TK, Geijsen N, Coffey PJ, Gadella BM, Verkleij AJ, van der Sluijs P et al (2004) Phosphatidylinositol 4-kinasebeta is critical for functional association of rab11 with the Golgi complex. *Mol Biol Cell* 15: 2038–2047
- Greninger AL, Knudsen GM, Betegon M, Burlingame AL, DeRisi JL (2013) ACBD3 interaction with TBC1 domain 22 protein is differentially affected by enteroviral and kobuviral 3A protein binding. *MBio* 4: e00098-38
- Gu Z, Eils R, Schlesner M (2016) Complex heatmaps reveal patterns and correlations in multidimensional genomic data. *Bioinformatics* 32: 2847–2849
- Gupta GD, Coyaud E, Goncalves J, Mojarad BA, Liu Y, Wu Q, Gheiratmand L, Comartin D, Tkach JM, Cheung SW et al (2015) A dynamic protein interaction landscape of the human centrosome-cilium Interface. *Cell* 163: 1484–1499
- Hammond SM, Jenco JM, Nakashima S, Cadwallader K, Gu Q, Cook S, Nozawa Y, Prestwich GD, Frohman MA, Morris AJ (1997) Characterization of two alternately spliced forms of phospholipase D1. Activation of the purified enzymes by phosphatidylinositol 4,5-bisphosphate, ADP-ribosylation factor, and rho family monomeric GTP-binding proteins and protein kinase C-alpha. *J Biol Chem* 272: 3860–3868
- Hammond GR, Machner MP, Balla T (2014) A novel probe for phosphatidylinositol 4-phosphate reveals multiple pools beyond the Golgi. *J Cell Biol* 205: 113–126
- Hsu NY, Illytska O, Belov G, Santiana M, Chen YH, Takvorian PM, Pau C, van der Schaar H, Kaushik-Basu N, Balla T et al (2010) Viral reorganization of the secretory pathway generates distinct organelles for RNA replication. *Cell* 141: 799–811
- Huttlin EL, Bruckner RJ, Navarrete-Perea J, Cannon JR, Baltier K, Gebreab F, Gygi MP, Thornock A, Zarraga G, Tam S et al (2021) Dual proteome-scale networks reveal cell-specific remodeling of the human interactome. *Cell* 184: 3022–3040 e3028
- Iglesias NG, Mondotte JA, Byk LA, De Maio FA, Samsa MM, Alvarez C, Gamarnik AV (2015) Dengue virus uses a non-canonical function of the host GBF1-Arf-COPI system for capsid protein accumulation on lipid droplets. *Traffic* 16: 962–977
- Jang JH, Lee CS, Hwang D, Ryu SH (2012) Understanding of the roles of phospholipase D and phosphatidic acid through their binding partners. *Prog Lipid Res* 51: 71–81
- Jenkins GM, Frohman MA (2005) Phospholipase D: a lipid centric review. *Cell Mol Life Sci* 62: 2305–2316
- Kahn RA, Gilman AG (1986) The protein cofactor necessary for ADP-ribosylation of Gs by cholera toxin is itself a GTP binding protein. *J Biol Chem* 261: 7906–7911
- Lahrouchi N, Postma AV, Salazar CM, De Laughter DM, Tjong F, Piherova L, Bowling FZ, Zimmerman D, Lodder EM, Ta-Shma A et al (2021) Biallelic loss-of-function variants in PLD1 cause congenital right-sided cardiac valve defects and neonatal cardiomyopathy. *J Clin Invest* 131: e142148
- Janke KH, van der Schaar HM, Belov GA, Feng Q, Duijings D, Jackson CL, Ehrenfeld E, van Kuppeveld FJ (2009) GBF1, a guanine nucleotide exchange factor for Arf, is crucial for coxsackievirus B3 RNA replication. *J Virol* 83: 11940–11949
- Li Y, Ling K, Hu J (2012) The emerging role of Arf/Arl small GTPases in cilia and ciliopathies. *J Cell Biochem* 113: 2201–2207
- Liu MY, Gutowski S, Sternweis PC (2001) The C terminus of mammalian phospholipase D is required for catalytic activity. *J Biol Chem* 276: 5556–5562
- Massenburg D, Han JS, Liyanage M, Patton WA, Rhee SG, Moss J, Vaughan M (1994) Activation of rat brain phospholipase D by ADP-ribosylation factors 1,5, and 6: Separation of ADP-ribosylation factor-dependent and oleate-dependent enzymes. *Proc Natl Acad Sci U S A* 91: 11718–11722
- Miyamoto T, Han SI, Shimano H (2021) Protocol for rapid manipulation of mitochondrial morphology in living cells using inducible counter mitochondrial morphology (iCMM). *STAR Protoc* 2: 100721
- Mizuno-Yamasaki E, Rivera-Molina F, Novick P (2012) GTPase networks in membrane traffic. *Annu Rev Biochem* 81: 637–659
- Nishikiori M, Mori M, Dohi K, Okamura H, Katoh E, Naito S, Meshi T, Ishikawa M (2011) A host small GTP-binding protein ARL8 plays crucial roles in tobamovirus RNA replication. *PLoS Pathog* 7: e1002409
- Noakes CJ, Lee G, Lowe M (2011) The PH domain proteins IPIP2A and B link OCRL1 to receptor recycling in the endocytic pathway. *Mol Biol Cell* 22: 606–623
- Park SY, Guo X (2014) Adaptor protein complexes and intracellular transport. *Biosci Rep* 34: e00123
- Prakash P, Gofe AA (2017) Membrane orientation dynamics of lipid-modified small GTPases. *Small GTPases* 8: 129–138
- Pucadyil TJ, Schmid SL (2009) Conserved functions of membrane active GTPases in coated vesicle formation. *Science* 325: 1217–1220
- Raudvere U, Kolberg L, Kuzmin I, Arak T, Adler P, Peterson H, Vilo J (2019) G: Profiler: a web server for functional enrichment analysis and conversions of gene lists (2019 update). *Nucleic Acids Res* 47: W191–W198
- Rojas AM, Fuentes G, Rausell A, Valencia A (2012) The Ras protein superfamily: evolutionary tree and role of conserved amino acids. *J Cell Biol* 196: 189–201
- Rosa-Ferreira C, Christis C, Torres IL, Munro S (2015) The small G protein Arl5 contributes to endosome-to-Golgi traffic by aiding the recruitment of the GARP complex to the Golgi. *Biol Open* 4: 474–481
- Roux KJ, Kim DI, Burke B, May DG (2018) BioID: a screen for protein-protein interactions. *Curr Protoc Protein Sci* 91: 19.23.11–19.23.15
- Sanger A, Hirst J, Davies AK, Robinson MS (2019) Adaptor protein complexes and disease at a glance. *J Cell Sci* 132: jcs222992
- Santiago-Tirado FH, Bretscher A (2011) Membrane-trafficking sorting hubs: cooperation between PI4P and small GTPases at the trans-Golgi network. *Trends Cell Biol* 21: 515–525
- Sasaki J, Ishikawa K, Arita M, Taniguchi K (2012) ACBD3-mediated recruitment of PI4KB to picornavirus RNA replication sites. *EMBO J* 31: 754–766
- Seixas E, Barros M, Seabra MC, Barral DC (2013) Rab and Arf proteins in genetic diseases. *Traffic* 14: 871–885
- Selvy PE, Lavieri RR, Lindsley CW, Brown HA (2011) Phospholipase D: enzymology, functionality, and chemical modulation. *Chem Rev* 111: 6064–6119
- Siltanen S, Syrjakoski K, Fagerholm R, Ikonen T, Lipman P, Mallott J, Holli K, Tammela TL, Jarvinen HJ, Mecklin JP et al (2008) ARLTS1 germline variants and the risk for breast, prostate, and colorectal cancer. *Eur J Hum Genet* 16: 983–991
- Sung TC, Zhang Y, Morris AJ, Frohman MA (1999) Structural analysis of human phospholipase D1. *J Biol Chem* 274: 3659–3666
- Supek F, Bosnjak M, Skunca N, Smuc T (2011) REVIGO summarizes and visualizes long lists of gene ontology terms. *PLoS One* 6: e21800
- Tai AW, Bojjireddy N, Balla T (2011) A homogeneous and nonisotopic assay for phosphatidylinositol 4-kinases. *Anal Biochem* 417: 97–102

- Tannous BA (2009) Gaussia luciferase reporter assay for monitoring biological processes in culture and *in vivo*. *Nat Protoc* 4: 582–591
- Thompson A, Schafer J, Kuhn K, Kienle S, Schwarz J, Schmidt G, Neumann T, Johnstone R, Mohammed AK, Hamon C (2003) Tandem mass tags: a novel quantification strategy for comparative analysis of complex protein mixtures by MS/MS. *Anal Chem* 75: 1895–1904
- Uhlen M, Oksvold P, Fagerberg L, Lundberg E, Jonasson K, Forsberg M, Zwahlen M, Kampf C, Wester K, Hober S et al (2010) Towards a knowledge-based human protein atlas. *Nat Biotechnol* 28: 1248–1250
- Uhlen M, Fagerberg L, Hallstrom BM, Lindskog C, Oksvold P, Mardinoglu A, Sivertsson A, Kampf C, Sjostedt E, Asplund A et al (2015) Proteomics. tissue-based map of the human proteome. *Science* 347: 1260419
- Wasiak S, Legendre-Guillemain V, Puertollano R, Blondeau F, Girard M, de Heuvel E, Boismenu D, Bell AW, Bonifacino JS, McPherson PS (2002) Enthoprotin: A novel clathrin-associated protein identified through subcellular proteomics. *J Cell Biol* 158: 855–862
- Williams C, Choudhury R, McKenzie E, Lowe M (2007) Targeting of the type II inositol polyphosphate 5-phosphatase INPP5B to the early secretory pathway. *J Cell Sci* 120: 3941–3951
- Yamazaki M, Zhang Y, Watanabe H, Yokozeki T, Ohno S, Kaibuchi K, Shibata H, Mukai H, Ono Y, Frohman MA et al (1999) Interaction of the small G protein RhoA with the C terminus of human phospholipase D1. *J Biol Chem* 274: 6035–6038
- Youn JY, Dunham WH, Hong SJ, Knight JDR, Bashkurov M, Chen GI, Bagci H, Rathod B, MacLeod G, Eng SWM et al (2018) High-density proximity mapping reveals the subcellular organization of mRNA-associated granules and bodies. *Mol Cell* 69: 517–532.e511
- Zewe JP, Miller AM, Sangappa S, Wills RC, Goulden BD, Hammond GRV (2020) Probing the subcellular distribution of phosphatidylinositol reveals a surprising lack at the plasma membrane. *J Cell Biol* 219: e201906127
- Zhang L, Elias JE (2017) Relative protein quantification using tandem mass tag mass spectrometry. *Methods Mol Biol* 1550: 185–198